

# Immunocompatible elastomer with increased resistance to the foreign body response

Received: 14 May 2024

Accepted: 23 August 2024

Published online: 30 August 2024

 Check for updates

Xianchi Zhou<sup>1,2</sup>, Zhouyu Lu<sup>3</sup>, Wenzhong Cao<sup>2</sup>, Zihao Zhu<sup>2</sup>, Yifeng Chen<sup>2</sup>, Yanwen Ni<sup>2</sup>, Zuolong Liu<sup>1,2</sup>, Fan Jia<sup>4</sup>, Yang Ye<sup>3</sup>, Haijie Han<sup>3</sup>, Ke Yao<sup>3</sup>, Weifeng Liu<sup>5</sup>, Youxiang Wang<sup>2</sup>, Jian Ji<sup>1,2</sup> & Peng Zhang<sup>1,2</sup> ✉

Polymeric elastomers are extensively employed to fabricate implantable medical devices. However, implantation of the elastomers can induce a strong immune rejection known as the foreign body response (FBR), diminishing their efficacy. Herein, we present a group of immunocompatible elastomers, termed easy-to-synthesize vinyl-based anti-FBR dense elastomers (EVADE). EVADE materials effectively suppress the inflammation and capsule formation in subcutaneous models of rodents and non-human primates for at least one year and two months, respectively. Implantation of EVADE materials significantly reduces the expression of inflammation-related proteins S100A8/A9 in adjacent tissues compared to polydimethylsiloxane. We also show that inhibition or knockout of S100A8/A9 leads to substantial attenuation of fibrosis in mice, suggesting a target for fibrosis inhibition. Continuous subcutaneous insulin infusion (CSII) catheters constructed from EVADE elastomers demonstrate significantly improved longevity and performance compared to commercial catheters. The EVADE materials reported here may enhance and extend function in various medical devices by resisting the local immune responses.

Polymeric elastomers are extensively employed in manufacturing biomedical devices designed for short-term and long-term implantation within the body<sup>1–4</sup>. For instance, poly(dimethylsiloxane) (PDMS) and thermoplastic polyurethane (TPU) serve as foundational materials for numerous medical implants, encompassing brain-machine interfaces<sup>5</sup>, cardiac pacemakers<sup>6,7</sup>, insulin infusion catheters<sup>8</sup>, cochlear implants<sup>9</sup>, drug-releasing devices<sup>10</sup>, and prostheses for medical aesthetics<sup>11,12</sup>. However, such polymer materials can elicit host recognition and instigate a cascade of immune-mediated foreign body response (FBR)<sup>13–20</sup>. The infiltration of immune cells, intense inflammatory responses,

fibrosis, and the subsequent formation of dense fibrous capsules during FBR can isolate the implants from the host, significantly impeding the functionality of biomaterials and the signal fidelity of implanted biomedical devices<sup>21–31</sup>. In clinical practice, the durability of biomedical implants is constrained by severe FBR induced by materials, often culminating in implant failure and eventual rejection. Approximately 90% of all failures in commonly employed medical devices can be attributed to the FBR, with as many as 30% of implantable devices experiencing failure during their operational lifespan<sup>32</sup>. For instance, patients with silicone breast implants may necessitate replacement within

<sup>1</sup>State Key Laboratory of Transvascular Implantation Devices, The Second Affiliated Hospital, Zhejiang University School of Medicine, Hangzhou, P. R. China.

<sup>2</sup>MOE Key Laboratory of Macromolecule Synthesis and Functionalization of Ministry of Education, Department of Polymer Science and Engineering, Zhejiang University, Hangzhou, P. R. China. <sup>3</sup>Eye Center, The Second Affiliated Hospital, School of Medicine, Zhejiang University, Zhejiang Provincial Key Laboratory of Ophthalmology, Zhejiang Provincial Clinical Research Center for Eye Diseases, Zhejiang Provincial Engineering Institute on Eye Diseases, Zhejiang University, Hangzhou, P. R. China. <sup>4</sup>Key Laboratory of Cardiovascular Intervention and Regenerative Medicine of Zhejiang Province, Department of Cardiology, Sir Run Run Shaw Hospital, School of Medicine, Zhejiang University, Hangzhou, P. R. China. <sup>5</sup>Department of Hepatobiliary and Pancreatic Surgery, The Second Affiliated Hospital, School of Medicine, Zhejiang University, Hangzhou, P. R. China. ✉e-mail: [zhangp7@zju.edu.cn](mailto:zhangp7@zju.edu.cn)

10–20 years due to capsule contracture induced by intense FBR while also bearing a certain risk of cancer<sup>11</sup>. In the context of insulin pumps, inflammation and fibrotic responses induced by subcutaneously implanted infusion catheters present challenges by hindering insulin absorption, necessitating replacement every 2–3 days<sup>8</sup>. These immune-driven fibrotic reactions not only cause pain and discomfort but also lead to device failure and additional costs. Mitigating the FBR of polymeric elastomers remains a significant challenge owing to their inherent hydrophobic nature and dense material interface<sup>33</sup>.

To address the challenges posed by the FBR in medical devices, attempts focus on developing biocompatible surface coatings on elastomer substrates. Various coatings have been reported to mitigate the FBR caused by the substrate, including drug-eluting coatings<sup>34,35</sup>, zwitterionic polymer coatings<sup>36,37</sup>, self-mimicking coatings<sup>13,38</sup>, and bioactive polymer coatings<sup>39,40</sup>. Recent studies showed that a coating derived from tetrahydropyran phenyl triazole (THPT) effectively mitigated the capsule formation against PDMS devices and silicone prosthesis<sup>12,39,40</sup>, although its synthesis is complicated. The successful transformation and application of biocompatible coatings in clinical practice have been scarce. Several challenges impede their widespread application. Firstly, the scarcity of materials with long-lasting anti-FBR properties persists<sup>41–43</sup>, with some necessitating complex chemical synthesis and purification processes. Secondly, the complicated coating procedures are unsuitable for large-scale industrial production. Thirdly, uneven coating application and inadequate coverage further hinder their efficacy. Lastly, the issue of coating detachment from substrates in complex physiological environments presents a formidable challenge.

An elastomer with intrinsic FBR resistance is of great interest for implantable devices. Herein, we report an elastomeric material platform termed easy-to-synthesize vinyl-based anti-FBR dense elastomers (EVADE). Inspired by the THPT group's effectiveness in regulating the FBR of elastomers, we speculate that the simpler structure of the tetrahydropyran ring may be a key component in THPT. Therefore, we design EVADE elastomers composed of poly(meth)acrylates, copolymerized mainly from the monomers 2-((tetrahydro-2H-pyran-2-yl)oxy) ethyl methacrylate (HPEMA) and octadecyl acrylate (ODA). By modifying the ratio of these monomers, the mechanical properties of EVADE materials can be tailored. Without any coatings, EVADE demonstrates negligible inflammation response upon implantation and exhibited minimal capsule formation when subcutaneously implanted in C57BL/6 mice for a year. Notably, the anti-fibrotic ability of EVADE is also verified in non-human primate (NHP) cynomolgus monkeys that mimic FBR observed in humans<sup>44</sup>. Our mechanistic study found that EVADE implants lead to significantly reduced expression of S100A8/A9 alarmins compared to PDMS. Additional inhibitory and knockout experiments confirm the importance of S100A8/A9 in the cascade of fibrotic tissue formation. Taking advantage of the superior immunocompatibility, insulin infusion catheters made from EVADE elastomers show significantly improved longevity and performance than commercial catheters.

## Results

### Design and characterization of EVADE materials

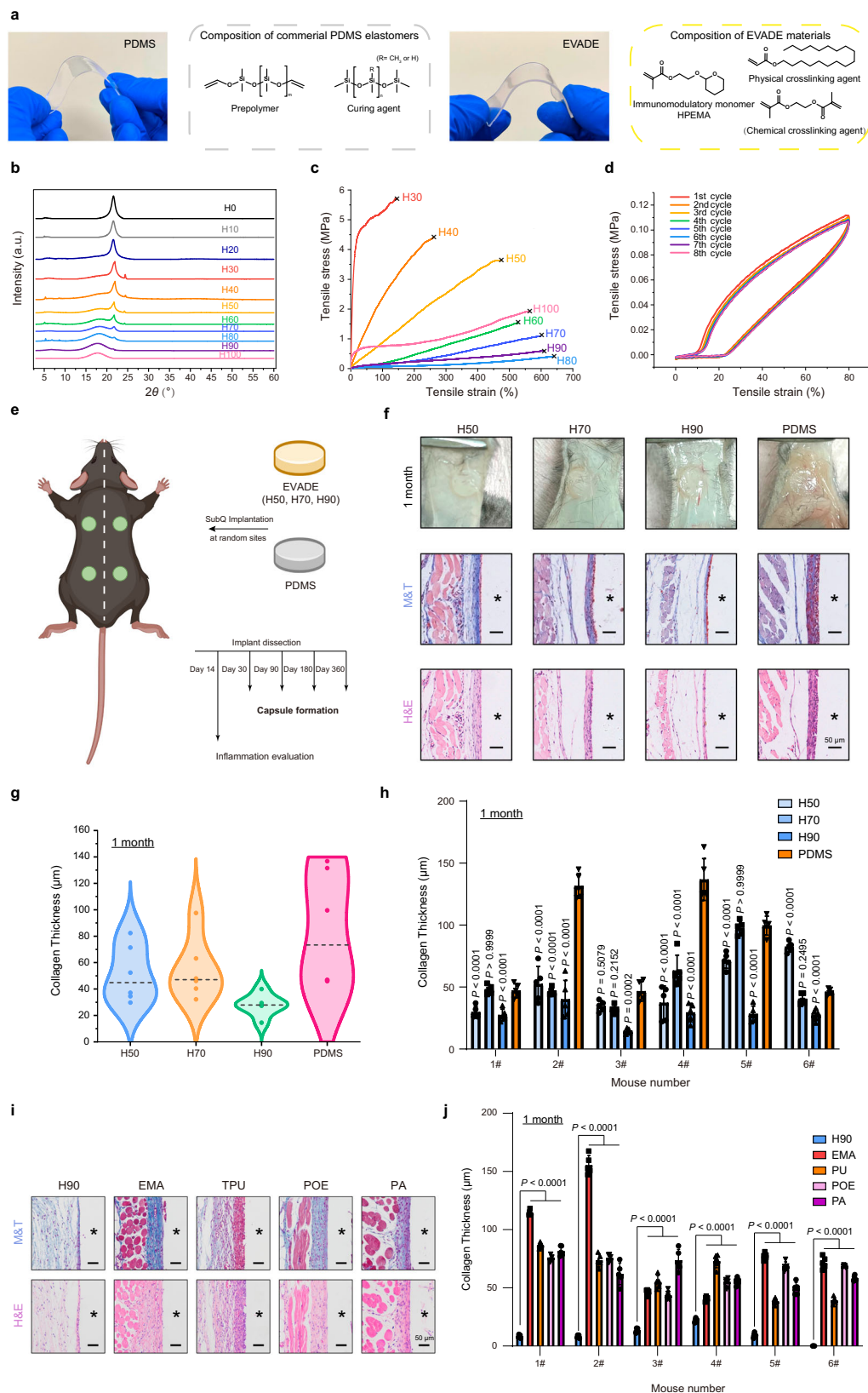
EVADE materials are based on a tetrahydropyran ether-derived methacrylate monomer HPEMA (Fig. 1a and Supplementary Figs. 1, 2). The monomer is easy to synthesize and can be facilely polymerized by free radical polymerization. To introduce physically cross-linkable moieties to the polymer structure, we copolymerized HPEMA with octadecyl acrylate (ODA), which has a long alkyl chain that can form microcrystals within the copolymers. The copolymers are made via bulk polymerization and named after the mole fraction of HPEMA, with an example being that a copolymer composed of 90 mol% HPEMA and 10 mol% ODA is designated as H90 (Supplementary Table 1). The characterizations of the series of copolymers are shown in Fig. 1b, and

Supplementary Figs. 3–6. X-ray diffraction (XRD) spectra proved that the long alkyl chain of ODA units forms a crystalline phase (Fig. 1b), which can serve as the crosslinking domains in the amorphous continuous phase for the elastomers. The mechanical performance of the EVADE materials was tested by tensile tests (Fig. 1c and Supplementary Fig. 7). When the content of HPEMA is more than 50%, the materials demonstrated very high fracture tensile strains of 500% or beyond. The tensile modulus of H60–H90 is in the range of 0.1–0.5 MPa, and the fracture stress is within 0.8–2.5 MPa. Note that the pure poly(HPEMA) (H100) has a high modulus at room temperature, due to its relatively higher glass transition temperature (Supplementary Figs. 3, 4). The cyclic tensile test of H90 showed typical elastomeric behavior (Fig. 1d). Similar to other thermoplastic elastomers, physical crosslinking restricts the relative motion of polymer chains but maintains enough freedom for segments to enable elasticity in the material. Note that adding a tiny amount of chemical crosslinkers can further adjust the mechanical performance. As shown in Supplementary Fig. 8, adding less than 1 wt% of ethylene glycol dimethacrylate (EGDMA) dramatically increases modulus and fracture stress at the expense of decreased fracture strain.

We selected three samples, H50, H70, and H90, for further tests. Before *in vivo* implantation to evaluate fibrotic reactions, the biocompatibility of these materials was first confirmed by cytotoxicity measurements of their extracts (Supplementary Fig. 9). One of the most commonly used medical elastomer, PDMS, was used for comparison for implantation studies. It is well-known that the specimen's physical properties, including modulus<sup>17,45</sup>, surface roughness<sup>11</sup>, and even size and shape<sup>46</sup>, affect the degree of fibrosis. To minimize these undesired influences, we adjusted the modulus of PDMS control samples to a similar value as H90 (~0.21 MPa, Supplementary Fig. 10). The surface topology, size, and shape of these sample discs were all kept similar (Supplementary Figs. 11–13). The subcutaneous (SC) implantation tests were conducted on C57BL/6 mice, with each mouse receiving implants of all four samples on its back (Fig. 1e). The discs were taken out one month after implantation. The representative photos and histological images are shown in Fig. 1f. Despite the notable inter-mouse variability (Fig. 1g), histological staining (Masson's trichrome and hematoxylin and eosin (H&E)) revealed that the EVADE materials, especially H90, showed a 10- to 40- $\mu$ m-thick fibrotic capsule, whereas this was 45–135  $\mu$ m for PDMS implants (Fig. 1f, h). It is worth noting that, in all six mice, the capsule surrounding the H90 implant was significantly thinner than that of the PDMS implant placed in the same animal. A comparative study was performed between H90 and four other most commonly used polymers for implants, including ethylene-(methyl acrylate) copolymer (EMA), TPU, poly(olefin) olefin (POE), and polyamide (PA). As shown in Fig. 1i, j, the implantation of H90 triggered negligible capsule formation, while all other materials exhibited a 35- to 160- $\mu$ m-thick fibrotic capsule, indicating the superior immunocompatibility of the EVADE materials.

### EVADE materials elicited a negligible acute inflammatory response

We investigated the acute inflammatory response induced by the EVADE materials after subcutaneous implantation in C57BL/6 mice for two weeks and observed negligible inflammation induced by H90 (Fig. 2a–e). We first performed immunohistochemical sectioning of pro-inflammatory markers CCR-7, TNF- $\alpha$ , and IL-6 and anti-inflammatory marker IL-10 to evaluate the impact of elastomer implantation on the level of inflammation in surrounding tissues (Fig. 2a, b). The results indicate that PDMS substantially increases inflammatory markers at the interface between the elastomer and tissue. In contrast, the expression of inflammatory markers is significantly lower for EVADE materials, with H90 demonstrating the most prominent reduction (~1/6 to 1/8 fold of those observed in the tissue surrounding the PDMS elastomer). However, the expression



levels of the anti-inflammatory marker IL-10 are low and do not show significant differences between the EVADE and PDMS elastomers. Next, to systematically evaluate the inflammatory response elicited by implanted EVADE materials, we employed proteome profiler antibody arrays to test multiple inflammation-related cytokines and chemokines in tissues adjacent to the implants after 2-week

implantation, with a mock group without implantation as the control. As shown in Fig. 2c, d and Supplementary Fig. 14, the tissues surrounding the H90 implant expressed significantly lower levels of chemokines, inflammatory cytokines, interferon- $\gamma$  (IFN- $\gamma$ ), and colony-stimulating factors. Of note, a prior study has demonstrated that interleukin-17 (IL-17), a cytokine closely related to T cells, is

**Fig. 1 | Fabrication and performance of EVADE materials.** **a** Photograph showing the flexible sheet of PDMS and EVADE material (H90) and their corresponding chemical structure. **b** XRD analysis of EVADE materials with different HPHEMA proportions. **c** Stress-strain curves under room temperature. Sample width, 2 mm; thickness, 1 mm; gauge length, 12 mm. Stretching speed, 10 mm min<sup>-1</sup>. **d** Stress-strain curves of H90 in cyclic tensile tests (80% strain in successive stretching). Sample width, 2 mm; thickness, 1 mm; gauge length, 12 mm. Stretching speed, 5 mm min<sup>-1</sup>. **e** Discs made of PDMS and EVADE materials (H50, H70, and H90) with a diameter of 4 mm and a thickness of 1 mm were implanted subcutaneously (SubQ) on mouse backs. The tissue surrounding the implants was analyzed 14, 30, 90, 180, and 360 days post-implantation. Created with BioRender.com released under a Creative Commons Attribution-NonCommercial-NoDerivs 4.0 International license. **f** Digital photos, H&E-, and Masson's trichrome (M&T)-stained histological sections of excised tissue around PDMS and EVADE elastomers 1-month post-implantation (representative for  $n = 6$  biologically independent samples). The white

dashed circle represents the PDMS disc that is vague to the naked eye due to strong collagen capsule encapsulation after implantation. The asterisk sign "\*" in the section images denotes the original locations of the implants. Scale bar = 50  $\mu$ m. **g** Distribution of collagen capsule thickness measured by M&T staining induced by PDMS and EVADE elastomers. The dashed lines in each data group represent the average ( $n = 6$  mice per group). **h** Thickness of the collagen capsule induced by PDMS and EVADE elastomers in each mouse ( $n = 6$  biologically independent replicates, mean  $\pm$  s.d.). **i** H&E-, and Masson's trichrome (M&T)-stained histological sections of excised tissue around H90 and commonly used implantable elastomers 1-month post-implantation (representative for  $n = 6$  biologically independent samples). Scale bar = 50  $\mu$ m. **j** Thickness of the collagen capsule induced by H90 and commonly used implantable elastomers in each mouse ( $n = 6$  biologically independent replicates, mean  $\pm$  s.d.). Statistical significance was determined by one-way analysis of variance (ANOVA) with Bonferroni multiple comparison test.

closely associated with the FBR in adaptive immunity<sup>47,48</sup>. Interestingly, we observed that the expression levels of IL-17, as well as its upstream and downstream cytokines, including interleukin-7, interleukin-16, and interleukin-23, were notably reduced in the tissues surrounding the H90 implant compared to the PDMS group.

Macrophages are critical in orchestrating the inflammatory response and are considered an essential cell type in the conventional theory of FBR<sup>49,50</sup>. Considering this, we further investigated the effect of EVADE materials on macrophage behavior. F4/80 immunofluorescent staining disclosed that large numbers of macrophages were recruited near PDMS and H50 implants, whereas only a few were observed near H70. In contrast, almost no macrophages were observed around H90 implants at two weeks (Fig. 2e). We further investigated the acute effects of EVADE implants on various immune cells. H90 and PDMS elastomers were subcutaneously implanted in C57BL/6 mice for one week. Then, the cells from the space around implants were extracted for single-cell RNA-sequencing (scRNA-seq) analysis to examine the composition and gene expression of immune cells (Fig. 2f). Using k-means clustering of single-cell transcriptomes. Among eight cell types, we identified three major clusters corresponding to macrophages, dendritic cells, and T/Natural Killer cells (Supplementary Figs. 15 and 16a, b). These clusters could be visualized in uniform manifold approximation and projection (UMAP) plots (Fig. 2g, h). We observed differences in immune cell infiltration and recruitment between the H90 and PDMS elastomer implants (Fig. 2i). Specifically, the tissue around the PDMS implant showed a higher proportion of macrophages than that of the H90 implant and mock group. Gene analysis showed that the implantation of H90 triggered a widespread downregulation of inflammatory cytokines, chemokines, and colony-stimulating factors in immune cells (Fig. 2j and Supplementary Fig. 17). Interestingly, some adaptive immune-related genes, such as interleukin-17 receptor a, have also been downregulated in immune cells near H90. We used gene set enrichment analysis (GSEA) to assess whether these decreased transcripts corresponded to activation of gene sets and found strong downregulation of gene sets involved in T cell receptor signaling pathway and Th17 cell differentiation (Fig. 2k, l,  $P < 0.013$  and  $P < 0.044$ , respectively). These gene sets were not significantly increased in the H90 compared with the mock group ( $P > 0.05$ ). Our findings suggest that the mechanism by which EVADE materials reduce FBR may involve both innate immunity and adaptive immunity.

### EVADE materials elicit minor immunological and fibrotic responses

To gain a deeper understanding of the cellular components driving the fibrotic response around EVADE materials, investigated the recruitment of primary FBR-related cells at the tissue interface adjacent to the elastomer one month after subcutaneous implantation (Fig. 3a). Immunofluorescence staining for myofibroblasts ( $\alpha$ -smooth muscle

actin ( $\alpha$ -SMA)), T cells (CD3), and macrophages (F4/80) revealed that large numbers of fibroblasts, macrophages, and T cells were recruited to the PDMS-tissue interface, whereas H90 elastomers showed a low level of FBR-related cellular overgrowth. Next, we performed RNA-sequencing on tissues near elastomers 1-month post-implantation, using a mock group without implantation as the control (Fig. 3b–f and Supplementary Fig. 18). Under the condition of  $P < 0.05$ , the number of differentially expressed genes in the PDMS and mock groups was 109, while in the H90 and mock groups was only 6 (Fig. 3b, c), indicating a minor immune reaction induced by EVADE materials. Kyoto Encyclopedia of Genes and Genomes (KEGG) pathway enrichment analysis of the two groups showed that the changed genes of PDMS compared with mock were mainly concentrated in FBR-related pathways, such as inflammatory response and immune response. In contrast, the genes changed in H90 compared with the mock were not FBR-related (Fig. 3d–f). We conducted western blotting (WB) and quantitative polymerase chain reaction (qPCR) analysis to confirm the difference in the expression of the critical factors (Fig. 3g, h, Supplementary Fig. 19, Supplementary Table 3). FBR-associated and inflammatory response-related gene expressions, including interleukin-6 (*Il6*), interleukin-1 beta (*Il1b*), tumor necrosis factor-alpha (*Tnfa*), colony-stimulating factor 1 (*Csf1*), C-X-C motif chemokine ligand 13 (*Cxcl13*), transforming growth factor beta 1 (*Tgfb1*), and interleukin-17 (*Il17*) did not show a significant difference between the tissues surrounding H90 and normal tissues, while that around PDMS were all significantly upregulated. Considering the role of IL-17 in regulating the FBR, we further quantified the secretion of IL-17 after 1-month implantation using the enzyme-linked immunosorbent assay (ELISA, Supplementary Fig. 20), which showed consistent results with the WB and qPCR tests.

### S100A8/A9 inhibition reduces the fibrotic response against silicone implants

Protein adsorption serves as a crucial initial step in the FBR process. Investigating surface protein adsorption after early implantation of implants may provide a deeper understanding of the mechanism by which EVADE materials reduce FBR. We first tested the surface adsorption property of EVADE materials and PDMS for fibrinogen (Fg) in vitro (Supplementary Fig. 21). The results showed that there was no significant difference in the adsorption of fibrinogen between EVADE materials (H50, H70, and H90) and PDMS. In other words, the inhibitory effect of EVADE materials on FBR is not based on the resistance of nonspecific protein adsorption. Next, we identified the protein species adsorbed on the surface of H90 and PDMS at 24 h after implantation by proteomics (Fig. 4a–c). Within 24 h, albumin was the most adsorbed protein on the surfaces of PDMS and H90 materials (Fig. 4a, b). Among the proteins adsorbed on the surface of PDMS, inflammation-related proteins S100A8 and S100A9 accounted for a large proportion (7.2% and 13.1%, respectively) (Fig. 4a). The adsorption of the two proteins on the H90 surface was significantly lower (3.5% and 7.4%, respectively)

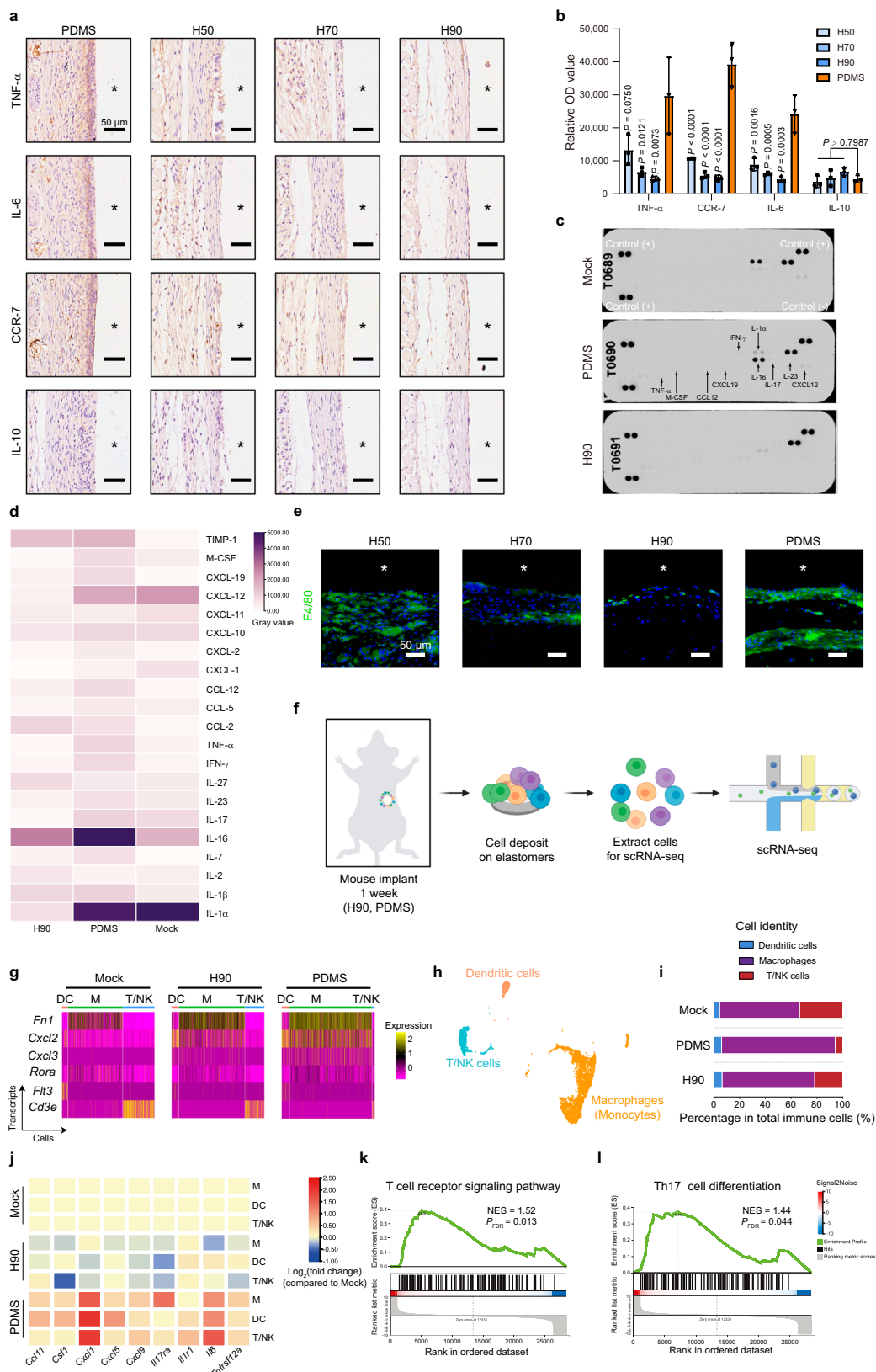


(Fig. 4b). S100A8/A9 protein was known to mediate the immune system through toll-like receptor 4 (TLR4) signaling, resulting in enhanced interleukin 17 (IL-17) expression<sup>51</sup>.

Comparing the protein intensities of PDMS and H90 surface adsorption, it was found that H90 had significantly lower S100A8 (0.33 folds) and S100A9 (0.38 folds) adsorption and higher Fga (3.42 folds)

and Fgb (4.38 folds) adsorption than PDMS (Fig. 4c). In the BP (biological process) analysis of KEGG, we found that the reduced proteins on H90 compared to PDMS are mainly concentrated in immune-related pathways, such as chronic inflammatory response, myeloid leukocyte migration, etc (Supplementary Fig. 22). Moreover, in MF (molecular function) analysis of KEGG, we found that H90

**Fig. 2 | EVADE materials suppress the acute inflammatory response against the implants. a, b** Discs made of PDMS and EVADE materials (H50, H70, and H90) with a diameter of 4 mm and a thickness of 1 mm were implanted SubQ on mouse backs. The tissue surrounding the implant was analyzed 14-day (a–e) or 7-day (f–i) post-implantation to evaluate the acute inflammation. Immunohistochemistry (IHC) was performed for inflammatory and anti-inflammatory markers (TNF- $\alpha$ , IL-6, CCR7, and IL-10) (staining shown in a, with quantification shown in b). Cells stained by inflammatory markers show a brown color, while all nuclei stained with hematoxylin are blue. Data were collected in the tissue within 50  $\mu$ m from the tissue-material interface ( $n = 3$  mice per group, mean  $\pm$  s.d.). Scale bar = 50  $\mu$ m. **c** Cytokine profiling for tissue lysates was run on one detection membrane per treatment group (from  $n = 3$  biological replicates), using the mock group without implantation as a control. The mouse cytokine array coordinates are shown in Supplementary Table 2. **d** Gray values of cytokine and chemokine expression. The maximum value of gray values is set to 5000, and colors will no longer deepen above 5000. **e** Immunofluorescence staining densities of F4/80 (represented by green staining). Counterstaining was performed with DAPI (blue) for cell nuclei. ( $n = 3$  mice per group). Scale bar = 50

$\mu$ m. **f** Preparation of immune cell populations one week after implanting EVADE and PDMS materials. Created with BioRender.com released under a Creative Commons Attribution-NonCommercial-NoDerivs 4.0 International license. **g** Single-cell transcriptional profiles clustered into groups by k-means clustering. DC dendritic cells; M macrophages; T/NK, T and natural killer cells. **h** UMAP embedding of individual immune cells pooled from all three samples (mock, PDMS, and H90). The resulting clusters are classified by immune cell type based on cell-specific expression profiles (Supplementary Fig. 15b). **i** Composition of peri-capsular immune cell identities recruited to each implant site. **j** Single-cell RNA-seq detection of cytokine and chemokine expression changes across individual immune cell populations. More detailed cytokine data are shown in Supplementary Fig. 16. **k, l** GSEA from T cell receptor signaling pathway (**k**) and Th17 cell differentiation (**l**) gene sets associated with expression changes in H90 versus PDMS implants. scRNA-seq was run on one sample pool per treatment group (from  $n = 3$  biological replicates). NES normalized enrichment score. Statistical significance was determined by one-way analysis of variance (ANOVA) with Bonferroni multiple comparison test.

downregulated the binding capacity of the receptor for advanced glycation endproducts (RAGE) receptor (Supplementary Fig. 23), which is one of the important inflammatory pathways downstream of S100A8 and S100A9<sup>52</sup>. From the RNA-seq and proteomic results above, we speculate that the expression and adsorption of S100A8/A9 protein may intensify the inflammatory response and further promote FBR in vivo.

S100A8/A9, which often exist in the form of heterodimers and have already been confirmed to play a decisive role in the development of inflammation<sup>53</sup>. We examined the expression of S100A8/A9 induced by implantation of EVADE and PDMS in adjacent tissues 24 h post-implantation using IHC and qPCR tests. IHC sections of S100A8 showed that short-term implantation of PDMS caused significant expression of S100A8 protein in neighboring tissues, while H90 hardly caused additional expression of S100A8 in vivo (Fig. 4d, e). qPCR analysis of S100A8 and S100A9 revealed similar trends as the IHC results (Fig. 4f). Additionally, we investigated the impact of EVADE material on macrophage behavior by incubating it with RAW264.7 cells in vitro. RNA-seq analysis of cell supernatant showed that H90 exhibited lower pro-inflammatory effects on macrophages than PDMS, as evidenced by the decrease in the secretion of inflammatory factors (IL-1 $\beta$ ) and chemokines (CXCL-2 and CXCL-3), as well as a reduction of the expression of S100A8 (Fig. 4g).

Despite numerous studies supporting the role of S100A8/A9 protein in inflammation response, there is no direct evidence indicating that inhibiting the expression of S100A8/A9 protein can mitigate the FBR of implants<sup>53</sup>. Considering our results, we hypothesized that inhibiting S100A8/A9 expression could potentially reduce the FBR against implants. We first tested the fibrotic response against PDMS discs to validate this hypothesis when the mice were given an S100A9 inhibitor tasquinimod (TAS). This orally active quinoline-3-carboxamide binds with high affinity to histone deacetylase 4 (HDAC4) and S100A9. TAS was given orally with daily drinking water at two doses (1 mg/kg and 3 mg/kg) to mice for 30 consecutive days after PDMS implantation (Fig. 4h–j). Masson sections showed significantly less collagen deposition around PDMS in the TAS group (the capsule thickness was  $\sim$ 1/2 to 1/3 fold of those observed without TAS administration), indicating inhibited FBR. In addition to the inhibitory model, we also constructed a S100A8-knockout (KO) mouse model by crossing Floxed-S100A8 transgenic (Tg) mice with LysM-Cre Tg mice (Supplementary Fig. 24). The model was validated using qRT-PCR and WB (Supplementary Fig. 25). PDMS discs were implanted subcutaneously for a month, with Cre- control mice as the control (Fig. 4k). Histological results showed that knocking out of S100A8 resulted in almost no fibrotic capsule formation (Fig. 4l, m). Furthermore, we confirmed the infiltration of FBR-related cells near the material through IHC. While implantation of PDMS in Cre- control mice caused

intense cell deposition, the implantation of PDMS in S100A8-knockout mice resulted in minor myofibroblasts recruitment (Fig. 4n, o). Additionally, PCR testing showed that knocking out the S100A8 gene significantly inhibits the expression of critical factors in FBR after PDMS implantation (Fig. 4p). Altogether, these findings suggest that S100A8/S100A9 proteins play a crucial role in the fibrosis process following material implantation, and reducing the expression of these proteins can alleviate the material-induced FBR.

### EVADE materials resist long-term FBR in mice and NHPs

The capability of biomaterials to resist long-term fibrous capsule formation is critical for maintaining the functionality of implantable devices in vivo. To evaluate this, we performed extended implantation studies, retrieving elastomer samples after three, six, and twelve months for fibrosis assessment. All H90 elastomer samples exhibited well-defined contours and were surrounded by thin fibrous capsules, as demonstrated by digital imaging and M&T staining (Fig. 5a–c and Supplementary Figs. 26–31). In contrast, control PDMS elastomers showed pronounced fibrosis after three months, developing a thick collagenous layer that rendered them entirely obscured at six and twelve months post-implantation. Analysis of capsule thickness indicated that the collagen layer around H90 remained stable three months post-implantation, while the layer surrounding PDMS continued to thicken for up to six months. To extend these findings to a higher-order species, we subcutaneously implanted H90 and PDMS elastomer discs in healthy cynomolgus monkeys (Fig. 5d). After two months, the implants were retrieved and analyzed. Masson's trichrome staining revealed a robust fibrous response in PDMS samples (up to 180  $\mu$ m), whereas H90 exhibited a thinner collagen layer (up to 60  $\mu$ m). Notably, no encapsulation was observed in two of the monkeys.

These findings suggest that EVADE materials can remarkably mitigate fibrous tissue responses within the NHP model (Fig. 5e, f). Finally, we performed RNA-seq analysis to profile the host-mediated immune recognition between subcutaneously implanted H90 and PDMS 2 months post-implantation (Fig. 5g). The results revealed noteworthy gene expression differences between groups with H90 elastomers and PDMS implants. Notably, H90 elastomers exhibited lower FBR-associated gene expression of the pro-inflammatory cytokine *IL1B* (which is typically associated with classically activated macrophages); monocyte and macrophage chemoattractants C-C motif chemokine ligand 2 (*CCL2*) and C-C motif chemokine ligand 3 (*CCL3*); T cell chemoattractants C-C motif chemokine ligand 22 (*CCL22*) and C-C motif chemokine ligand 24 (*CCL24*) compared with the PDMS implants. Our observations from this NHP study suggest that EVADE materials demonstrate a marked decrease in the secretion of pro-inflammatory cytokines, thereby provoking a host response that is notably less pronounced than the response triggered by silicone implants.

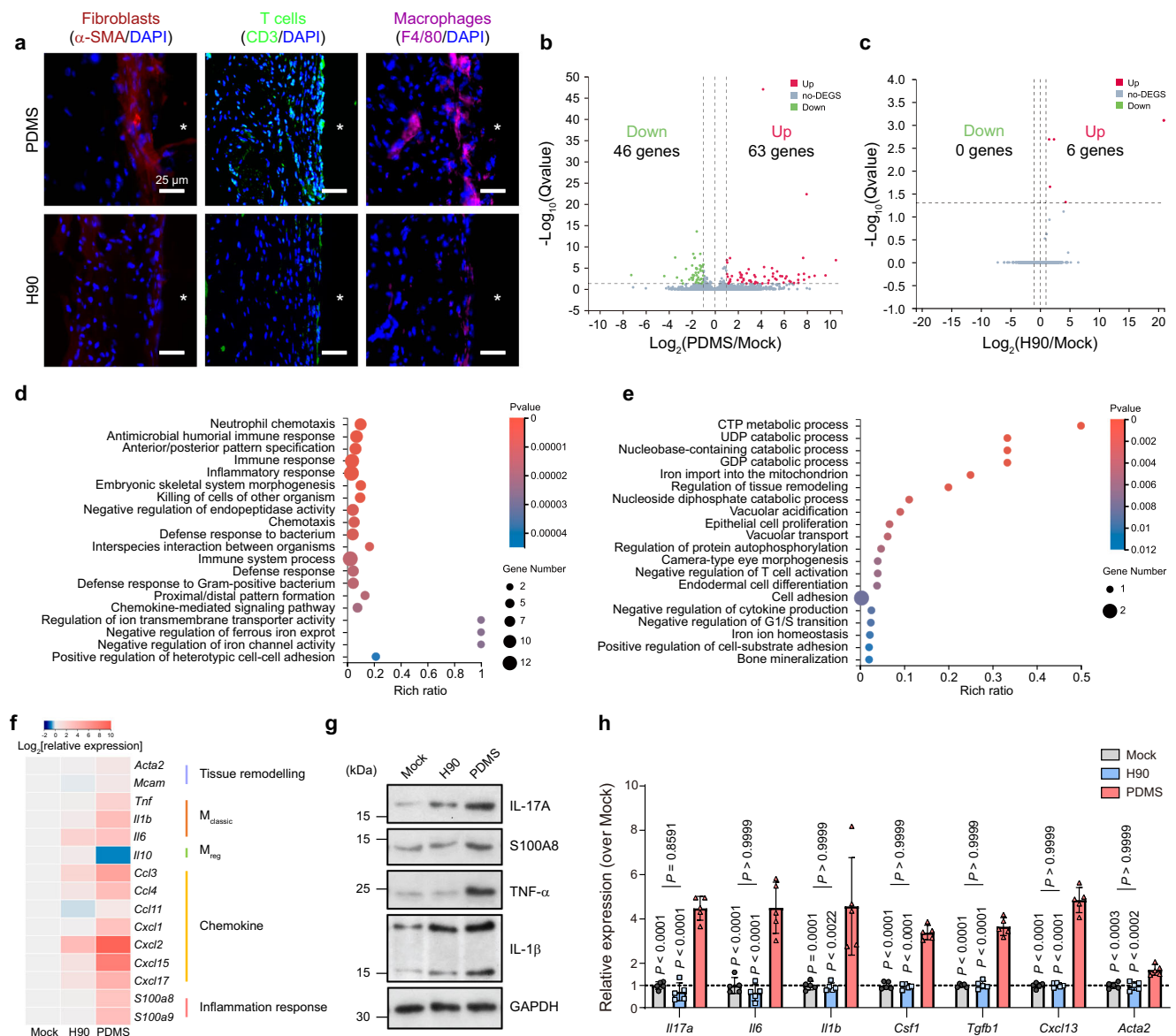


**Fig. 3 | Negligible immune response was elicited by the EVADE material implanted for one month.** Discs made of PDMS and H90 with a diameter of 4 mm and a thickness of 1 mm were implanted SubQ on mouse backs. The tissue surrounding the implant was analyzed 30 days post-implantation. Scale bar = 25  $\mu$ m. **a** Immunofluorescence staining of sections for  $\alpha$ -SMA (red, fibroblasts), CD3 (green, T cells), F4/80 (purple, macrophages), and nuclei stained via DAPI (blue) ( $n = 3$  mice per group). **b, c** Gene expression changes of PDMS/mock comparison (**b**) and H90/mock comparison (**c**). **d, e** KEGG pathway enrichment analysis of

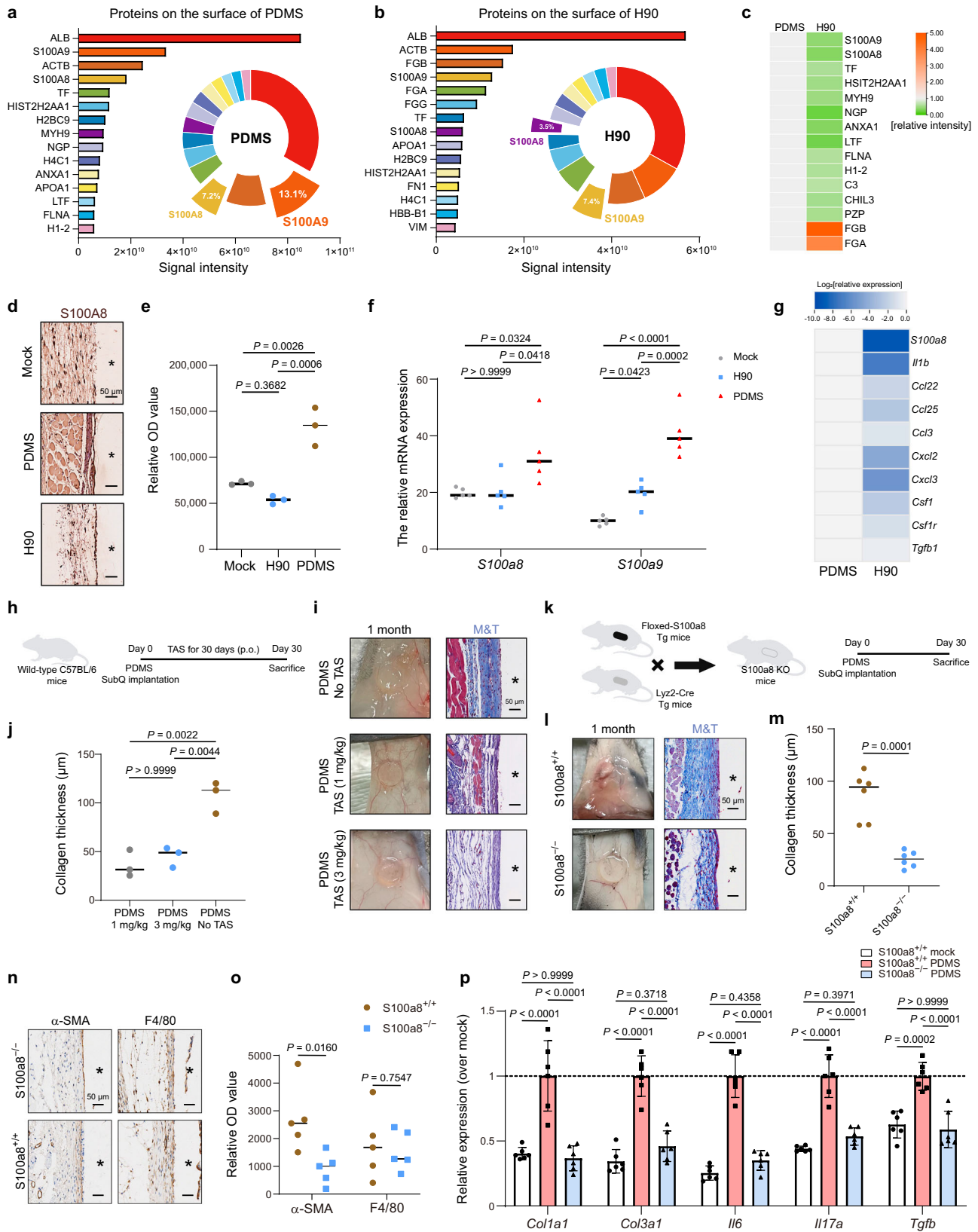
PDMS/mock comparison (**d**) and H90/mock comparison (**e**). **f** Gene expression analysis of phenotypic markers in tissues surrounding the H90 and PDMS materials, with data normalized to the mock group and presented on a  $\log_2$  scale ( $n = 3$  mice per group). **g** Semiquantitative western blot analysis of inflammatory and FBR-related factor expression in tissues surrounding the H90 and PDMS materials ( $n = 3$  mice per group). **h** qRT-PCR analysis of mRNA expression for FBR-related genes ( $n = 5$  mice per group, mean  $\pm$  s.d.). Statistical significance was determined by one-way analysis of variance (ANOVA) with Bonferroni multiple comparison test.

### Evaluation of EVADE CSII catheter under practical pump therapy conditions in diabetic mice

Our subcutaneous implantation studies conducted in murine and NHP models have yielded compelling evidence demonstrating the remarkably low inflammatory and fibrotic response elicited by EVADE elastomers post-implantation, especially when contrasted with other commercially utilized elastomers for the fabrication of biomedical devices. These findings highlight the outstanding anti-FBR performance of EVADE elastomers and underscore their potential applicability in practical medical device settings, promising improved in vivo performance by attenuating local immune reactions. To substantiate the translational significance of our observations, we employed a CSII pump model—a widely embraced therapeutic approach for managing both type 1 and type 2 diabetes. The inflammatory and fibrotic

response elicited post-implantation frequently compromises the practical efficacy of CSII catheters, leading to elevated occlusion rates and suboptimal glycemic control in clinical practice. This necessitates the replacement of devices every 2–3 days, posing a significant burden.

To address this challenge, we developed infusion catheters made from EVADE material and evaluated their performance under standard pump therapy conditions in a diabetic mouse model (Fig. 6a). EVADE-infused catheters were subcutaneously implanted in mice and secured with adhesive, while commercially available Silhouette catheters served as the control. To test the performance of EVADE catheters under natural micromotion, we connected the catheter to an infusion line and allowed the mice to carry the infusion set for up to 7 days. Following this, the catheter was linked to an insulin pump (Medtronic MiniMed 722) to assess functionality during continuous insulin infusion. Mice



received a continuous basal insulin infusion at a rate of 10  $\mu$ L/h, with additional bolus insulin infusions of 45  $\mu$ L each (Fig. 6b). On day 7 post-implantation, an insulin absorption assay was performed by administering a bolus infusion via the insulin pump. Insulin delivered through the Silhouette catheter showed a 0.5–1 h delay in absorption compared to standard subcutaneous (SC) administration, whereas

insulin delivered via the EVADE catheter exhibited a pharmacokinetic profile consistent with SC administration (Fig. 6c–e). Consequently, the EVADE infusion set produced a glycemic effect comparable to conventional SC insulin injection, as indicated by the minimum blood glucose level at 1-hour post-administration. In contrast, the Silhouette infusion set demonstrated a significant delay in pharmacological effect,



**Fig. 4 | S100A8/S100A9 inhibition reduces the fibrotic response to synthetic elastomers.** Discs made of PDMS with a diameter of 4 mm and a thickness of 1 mm were implanted SubQ on mouse backs. The tissue surrounding the implant was analyzed 24-hour (a–f) or 30-day (h–p) post-implantation. **a, b** Proteomic analysis of the protein lysates extracted from retrieved elastomers 24 h post-implantation, the various proteins on the surface of PDMS (**a**) and H90 (**b**) samples were sorted in descending order of protein mass spectrometry signal intensity (only the top 15 proteins with intensity were counted). The surface proportion of proteins with top 15 strength on PDMS (**a**) and H90 (**b**) is displayed in a circular graph. **c** Comparison of various protein intensities on the surfaces of PDMS and H90 (under the condition of ensuring equal total protein content). Proteomic analysis was run on one sample pool per treatment group (from  $n = 3$  biological replicates). IHC was performed for S100A8 (staining shown in **d**, with quantification shown in **e**). Cells stained by the S100A8 marker show a brown color. Data were collected in the tissue within 50  $\mu\text{m}$  from the tissue-material interface ( $n = 3$  mice per group, mean  $\pm$  s.d.). Scale bar = 50  $\mu\text{m}$ . **f** qRT-PCR analysis of mRNA expression for S100a8 and S100a9 ( $n = 5$  mice per group, mean  $\pm$  s.d.). **g** RNA profile in macrophages cultured on H90 and PDMS elastomers *ex vivo* for three days (under  $P < 0.05$ ). **h** The S100A9 inhibitor TAS (1 mg/kg or 3 mg/kg) was administered orally in drinking water to mice for 30 consecutive days with PDMS discs implanted four weeks previously.

**i, j** Digital photos and M&T-stained histological sections of excised 4-week post-implantation in wild-type mice (thickness of the collagen capsule shown in **j**,  $n = 3$  mice per group, mean  $\pm$  s.d.). The asterisk sign “\*” in the section images denotes the original locations of the implants. Scale bar = 50  $\mu\text{m}$ . **k** The construction and experimental overview of the S100A8-KO mice model. Created with BioRender.com released under a Creative Commons Attribution-NonCommercial-NoDerivs 4.0 International license. **l** Digital photos and M&T-stained histological sections of excised 4-week post-implantation in S100A8-KO mice (thickness of the collagen capsule shown in **m**,  $n = 6$  mice per group, mean  $\pm$  s.d.). The asterisk sign “\*” in the section images denotes the original locations of the implants. Scale bar = 50  $\mu\text{m}$ . **n** IHC was performed for FBR-related cell markers ( $\alpha$ -SMA for fibroblasts and F4/80 for macrophages) (staining shown in **n**, with quantification shown in **o**). Cells stained by inflammatory markers show a brown color, while all nuclei stained with hematoxylin are blue. Data were collected in the tissue within 50  $\mu\text{m}$  from the tissue-material interface ( $n = 5$  mice per group, mean  $\pm$  s.d.). **p** qRT-PCR analysis of mRNA expression for FBR-related genes in S100A8-KO mice ( $n = 6$  mice per group, mean  $\pm$  s.d.). Statistical significance was determined by one-way analysis of variance (ANOVA) with Bonferroni multiple comparison test (**e, f, j, p**) or unpaired, two-tailed *t*-test (**m, o**).

with the minimum blood glucose level occurring 0.5–1 hour later than in the EVADE group. We further assessed the long-term biocompatibility of these catheters by subcutaneously implanting them in mice for 30 days and performing histological analysis using Masson trichrome staining to evaluate fibrotic capsule formation (Fig. 6f). The Silhouette group exhibited excessive inflammatory cell infiltration and dense collagen encapsulation, which likely contributed to the observed occlusion or failure of insulin delivery. Conversely, the EVADE catheter displayed markedly less collagen deposition and a significantly reduced fibrotic capsule thickness, indicating a substantially mitigated FBR. These findings highlight the potential of EVADE material to improve the *in vivo* performance of implantable biomedical devices by reducing local immune responses.

## Discussion

In summary, we have developed coating-free immunocompatible elastomers with negligible inflammation and long-term resistance to fibrosis after implantation while being easy to synthesize and non-toxic. The mechanical properties of elastomers can be tailored within a broad range. Among them, H90, with the best performance, inhibited fibrosis in rodents and non-human primates for up to one year and two months, respectively. Compared to other elastomers commonly used in biomedical applications, H90 consistently displays outstanding anti-fibrotic properties. In exploring the underlying mechanism of the anti-fibrotic effect of the EVADE material, we found that it regulates both innate and adaptive immune responses triggered by the implantation. In addition, the expression level of S100A8/S100A9, an inflammation-related protein, was significantly lower in tissue around EVADE than the PDMS after implantation. Further S100A9 inhibition and S100A8-knockout studies confirmed that inhibiting the expression of S100A8/S100A9 protein can effectively reduce the FBR induced by material implantation. Lastly, we validated the practical application of EVADE elastomers in medical devices through a practical CSII model under pump therapy conditions. We believe that the immunocompatible elastomers described here will facilitate the development of both short-term and long-term implants for various biomedical applications.

## Methods

### Materials and reagents

2-Hydroxyethyl methacrylate (HEMA), 3,4-dihydro-2H-pyran, octadecyl acrylate (ODA), benzoyl peroxide (BPO), 3, 3', 5, 5'-tetramethylbenzidine (TMB), ammonium persulfate (APS), *N,N,N',N'*-tetramethyl ethylenediamine (TEMED), and *N,N'*-methylenebis(acrylamide) (MBAA) were supplied by Aladdin Reagent Co., Ltd. *o*-Phenylenediamine (OPD) and

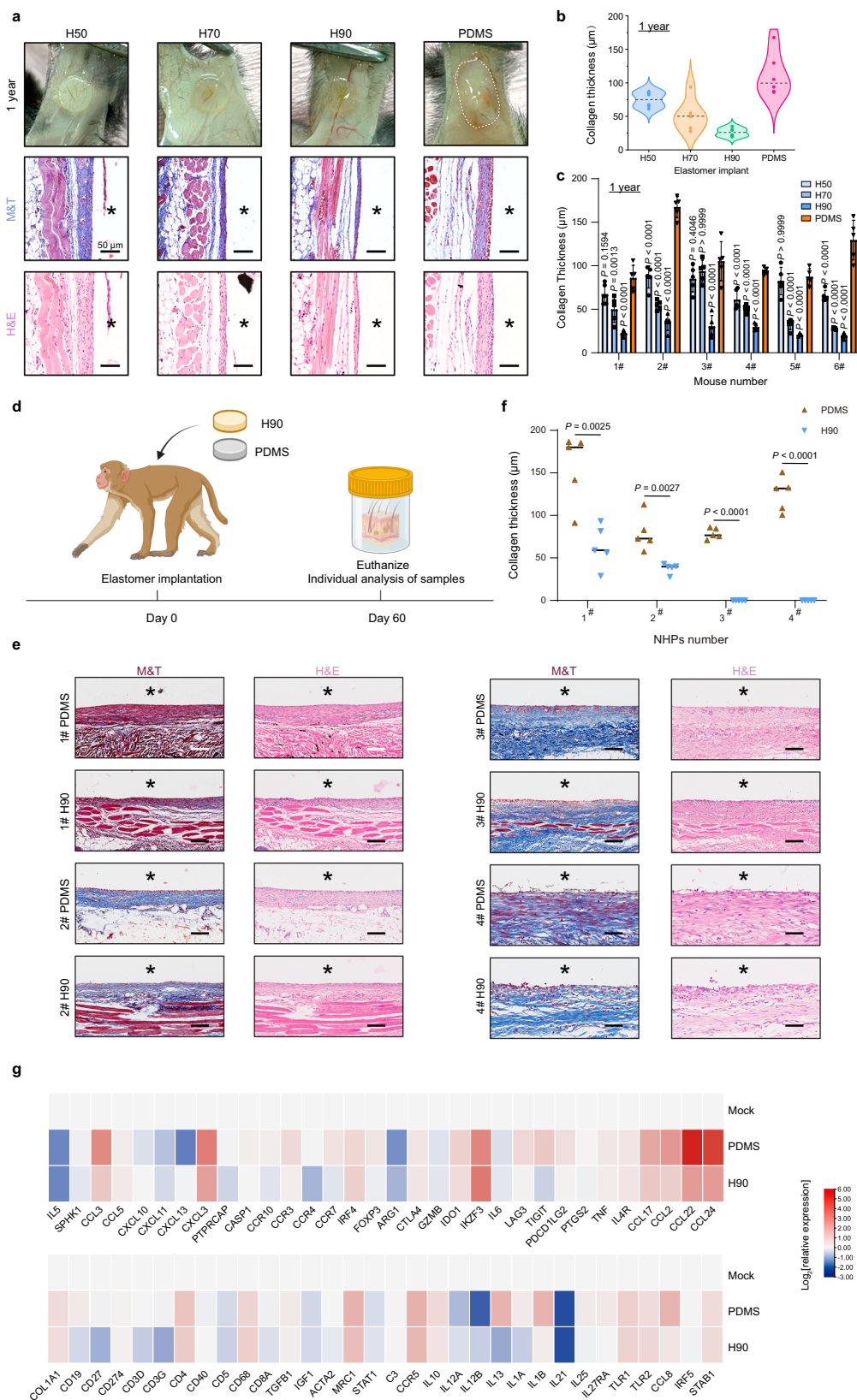
tasquinimod (TAS) were purchased from Macklin Reagent Co., Ltd. *p*-Toluenesulfonic acid (PTSA) was obtained from Rhawn Reagent Co., Ltd. Phosphate buffer solution (PBS) was purchased from Sangon Biotech Co., Ltd. The silicone elastomer Sylgard 184 was obtained from Dow Corning (catalog no. 3097358-1004). Fibrinogen, Ethylene glycol dimethacrylate (EGDMA), streptozocin (STZ), and 2-methacryloyloxyethyl phosphorylcholine (MPC) were purchased from Sigma-Aldrich. TPU (Lubrizol Pellethane 2363-80a), POE (ENGAGE 8999), PA (Pebax MED 6333), and EMA (LOTADER ax8900) were purchased from corresponding companies and processed into 1 mm thick sheets. The Silhouette infusion set (Silhouette Paradigm MMT-381A, MiniMed Reservoir (no. MMT-332A) and Medtronic MiniMed 722 pump were purchased from GEMCO Medical.

### Synthesis of HPHEMA monomers

2-((tetrahydro-2H-pyran-2-yl)oxy)ethyl methacrylate (HPHEMA) was synthesized as follows. To a stirred solution of HEMA (10 g, 1.0 eq.) in 30 mL of dry ether was added PTSA (1.3 g, 0.1 eq.). To this reaction mixture, a solution of 2,3-dihydropyran (10 mL, 1.4 eq.) in 5 mL dry ether was added dropwise at 0 °C. The reaction contents were warmed to room temperature and stirred in the dark for 3 h, concentrated and purified by column chromatography with ethyl acetate/hexane (1:4 v/v) to give the desired monomer as light-yellow oil in 87% yield (17.3 g). <sup>1</sup>H and <sup>13</sup>C NMR spectra were collected on a Bruker AVANCE III 500 spectrometer at 500 MHz and 125 MHz, respectively, using CDCl<sub>3</sub> as the solvent. <sup>1</sup>H NMR chemical shifts were referenced to the resonance for residual protonated solvent ( $\delta$  0.00 for TMS in CDCl<sub>3</sub>). <sup>13</sup>C NMR chemical shifts were referenced to the solvent ( $\delta$  77.16 for CDCl<sub>3</sub>). <sup>1</sup>H NMR (500 MHz, CDCl<sub>3</sub>)  $\delta$  6.07 (s, 1H), 5.52 (s, 1H), 4.60 (t,  $J = 3.4$  Hz, 1H), 4.39–4.26 (m, 2H), 3.95 (ddd,  $J = 11.3, 6.1, 3.7$  Hz, 1H), 3.91–3.80 (m, 1H), 3.69 (ddd,  $J = 11.3, 6.4, 3.7$  Hz, 1H), 3.57–3.45 (m, 1H), 1.96 (s, 3H), 1.89–1.77 (m, 1H), 1.76–1.66 (m, 1H), 1.57 (dddd,  $J = 14.0, 11.8, 10.1, 5.2, 4$  Hz). <sup>13</sup>C NMR (125 MHz, CDCl<sub>3</sub>)  $\delta$  167.38 (s), 136.24 (s), 125.64 (s), 98.67 (s), 65.10 (s), 63.89 (s), 61.94 (s), 30.45 (s), 25.41 (s), 19.19 (s), 18.32 (s). Mass spectra were acquired using an Agilent 6545 Q-TOF mass spectrometer. ESI-MS: [M + Na]<sup>+</sup>: 237.11.

### Fabrication and characterization of EVADE materials

The EVADE materials were fabricated by radical bulk copolymerization in Poly tetra fluoroethylene (PTFE) molds with the desired shape. A reaction mixture containing HPHEMA monomer, ODA monomer, and 0.5 wt% (relative to the total weight of monomers) of initiator BPO was thermo-polymerized using PTFE slides separated by a 1 mm thick PTFE spacer. The reaction was kept at 70 °C for 2 d.



After polymerization, the elastomer samples were soaked thoroughly until equilibrium in anhydrous ethanol to remove residual monomer, followed by drying under vacuum at room temperature for further tests. H90 elastomers crosslinked with EGDMA were synthesized using a similar procedure. The amount of EGDMA added is from 0 to 1 wt%. The chemical structures of these EVADE materials (H0 to H100,

10% as a step) were confirmed by <sup>1</sup>H NMR (400 MHz, CDCl<sub>3</sub>). The molecular structures of the EVADE materials were analyzed by Fourier Transform Infrared Spectroscopy (FTIR) using a Thermo Nicolet 6700 FT-IR Spectrometer with a Smart iTR Attenuated Total Reflectance (ATR). The wavenumber ranged from 500 to 4000 cm<sup>-1</sup> with 32 scans.

**Fig. 5 | Long-term anti-fibrotic efficacy of EVADE materials in mice and NHPs.** **a** Digital photos, H&E-, and M&T-stained histological sections of excised 1-year post-implantation in mice (representative for  $n = 6$  biologically independent samples). The white dashed circle represents the PDMS disc that is not visible to the naked eye due to strong collagen capsule encapsulation after implantation. The asterisk sign "\*" in the section images denotes the original locations of the implants. Scale bar = 50  $\mu\text{m}$ . **b** Distribution of collagen capsule thickness measured by M&T staining. The dashed lines in each data group represent the average ( $n = 6$  mice per group). **c** Thickness of the collagen capsule in each mouse ( $n = 6$  biologically independent replicates, mean  $\pm$  s.d.). **d** Schematic depicting the cynomolgus monkeys study design. Created with BioRender.com released under a Creative

Commons Attribution-NonCommercial-NoDerivs 4.0 International license. **e** H&E- and Masson's trichrome (M&T)-stained histological sections of excised SC tissue two months post-implantation in NHPs. The asterisk sign "\*" in the section images denotes the original locations of the implants. Scale bar = 200  $\mu\text{m}$ . **f** Quantified data of collagen capsule thickness of M&T staining in each monkey ( $n = 5$  section positions per monkey). **g** Gene expression analysis of phenotypic markers in tissues surrounding the H90 and PDMS materials two months post-implantation in NHPs, with data normalized to the mock group and presented on a  $\log_2$  scale ( $n = 3$  monkeys per group). Statistical significance was determined by one-way analysis of variance (ANOVA) with Bonferroni multiple comparison test (c) and an unpaired, two-tailed  $t$ -test (f).

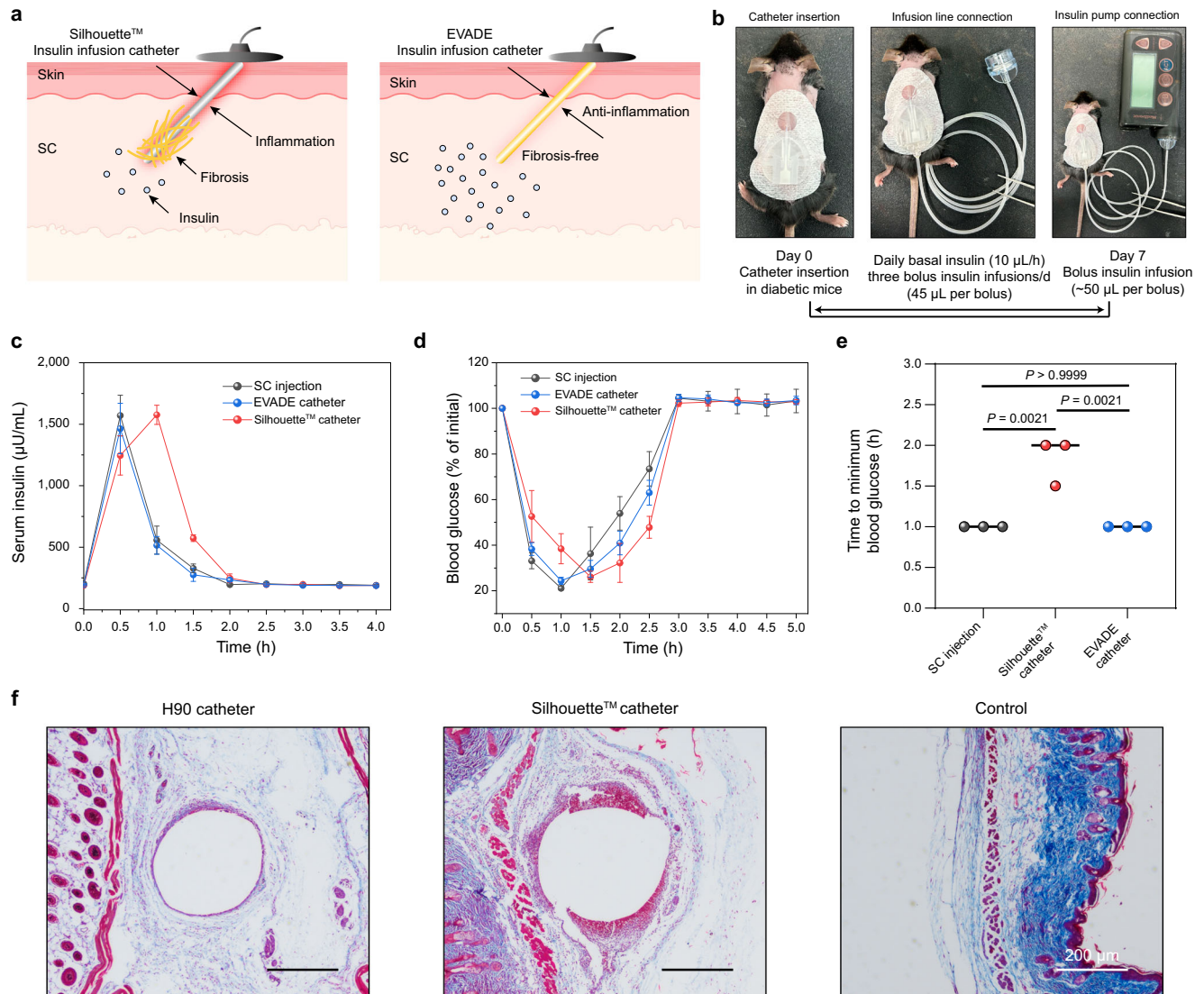


**Fig. 6 | Catheters made of EVADE elastomer retained long-term function in diabetic mice under practical pump therapy conditions.** **a** Schematic representation of CSII catheter made of EVADE elastomer enabling the long-term use of infusion catheter and faster insulin absorption. Created with BioRender.com released under a Creative Commons Attribution-NonCommercial-NoDerivs 4.0 International license. **b** SC infusion catheter insertion and insulin pump connection through infusion lines. **c, d, e** Plasma human insulin concentrations (c), Blood glucose (d), time to minimum blood glucose (e), after bolus insulin (4 IU/kg) was

infused via insulin pump seven days after SC catheter insertion. Mice receiving syringe-based SC insulin at the same dosage were used as control ( $n = 3$  mice, mean  $\pm$  s.d.). **f** Representative Masson trichrome-stained images of tissues surrounding SC-implanted catheters from different groups at days 30 post-implantation (representative for  $n = 2$  biologically independent samples). Scale bar = 200  $\mu\text{m}$ . Statistical significance was determined by one-way analysis of variance (ANOVA) with Bonferroni multiple comparison test.

**XRD.** The crystallization behavior of EVADE materials (H0 to H100, 10% as a step) was measured by Powder X-ray Diffractometer (Rigaku Ultima IV) with  $\text{Cu K}\alpha$  radiation in the  $2\theta$  range  $3\text{--}60^\circ$  with a step size of  $0.02^\circ$  (40 mA, 40 kV).

**DSC.** The  $T_g$ s of EVADE materials (H0 to H100, 10% as a step) were measured by DSC (Q20, TA instruments, New Castle, DE, USA) at a scanning range of  $-70$  to  $150^\circ\text{C}$  with a heating/cooling rate of  $10^\circ\text{C min}^{-1}$  and a nitrogen flow rate of  $50\text{ mL min}^{-1}$ . During the test, each

sample was heated to 150 °C, kept at 150 °C for 3 min to eliminate thermal history, cooled to -70 °C, and then heated to 150 °C again.  $T_g$  was taken as the inflection of the DSC curve.

**Mechanical tests.** Tensile tests were measured on a tensile-compressive mechanical tester (Zwick/Roell Z020) with a 500 N load cell at room temperature and 37 °C, respectively. For tensile tests, EVADE materials and PDMS were cut from the elastomer sheet into a dumbbell shape with an initial gauge length of 12 mm and a width of 2 mm. The stretch rate was 10 mm min<sup>-1</sup>, and the nominal stress and strain were recorded. Young's modulus of the elastomer was calculated from the initial slope of the tensile stress-strain curve with a strain below 10%. Average data were acquired by testing three specimens for each sample. The stress-strain curve of the EVADE elastomer (H90) in cyclic stress-strain tests (80% strain) in successive stretching was conducted using the same size samples as mentioned above, but the stretching speed was set as 5 mm min<sup>-1</sup>. The authors would like to thank Meifang Wang from Shiyanjia Lab ([www.shiyanjia.com](http://www.shiyanjia.com)) for providing the assistance with the mechanical tests.

**Preparation and modulus adjustment of PDMS.** PDMS elastomers were prepared and used as controls, with the ratio of prepolymer and curing agent adjusted to ensure a similar tensile modulus between PDMS and H90. The mixture was degassed and poured into plastic dishes at a fixed volume, resulting in a PDMS layer with a thickness of ~1 mm. The PDMS layer was cured at 80 °C for 2 h, peeled, and subsequently cleaned with ethanol and dried.

**Scanning electron microscope (SEM).** The elastomer samples were dried thoroughly under vacuum and then loaded on aluminum pellets using carbon tape. The samples were coated with a 2-nm gold layer using a sputter coating system, and images were recorded on a scanning electron microscope (Hitachi SU8010).

**Non-contact profilometry.** Samples with a diameter of 4 mm were cleaned with 99% isopropyl alcohol. On an anti-vibration table, the samples were placed under the ×20 lens of a non-contact profilometer (KEYENCE VR-5200). The samples were adjusted to ensure a 90° angle between the surface of interest and the lens, and images were focused. Smooth surfaces were acquired in automatic mode; however, if the topography was unknown, the upper and lower z-axis limits were manually adjusted. Using the confocal program visualization mode, the upper and lower z limits were set on the observed image with both focusing extremes appearing completely black. Next, program visualization was set to microscope mode, and brightness was adjusted to automatic, ensuring no areas appeared red due to overexposure. Images and measurements were then captured for each sample. Data were subsequently analyzed.

#### **Biocompatibility of EVADE materials**

Human primary umbilical vein endothelial cells (ECs) were isolated from human umbilical veins and arteries with approval from the local medical ethics committee. ECs were cultured in endothelial cell medium supplemented with 10% fetal bovine serum (FBS), 20 mg/mL endothelial cell growth supplement, 60 µg/mL penicillin, and 100 µg/mL streptomycin, maintained at 37 °C in a humidified atmosphere with 5% CO<sub>2</sub>.

**Extraction cytotoxicity test.** To assess cytotoxicity, endothelial cell medium extractions were prepared by immersing 600 mg of EVADE material in 3 mL of endothelial cell medium containing 10% FBS for 30 days. Cytotoxicity was evaluated using the Cell Counting Kit-8 (CCK-8) from Meilunbio (catalog no. MA0218). Endothelial cells were seeded at a density of 5000 cells per well in a 96-well plate and incubated overnight. The following day, the culture medium was replaced

with the prepared extraction medium. After 24 h of incubation, the medium was replaced with 200 µL of fresh medium containing 20 µL of CCK-8 and incubated for an additional 4 h. Cell viability was measured using a Bio-Rad microplate reader at 450 nm, with 570 nm as the reference wavelength. Cells cultured in standard endothelial cell medium served as controls. Data were averaged from five independent experiments.

#### **Modulation of the RNA profile in macrophages cultured on EVADE materials ex vivo**

Murine RAW264.7 macrophages were cultured in RPMI 1640 medium and cultured in the presence of 10% FBS in a humidified atmosphere with 5% CO<sub>2</sub> at 37 °C. EVADE materials and PDMS were cut into the size of a six-well plate well and then treated with 75% ethanol. Discard ethanol and let it evaporate until there is no residue. RAW264.7 cells were seeded in a 96-well plate at a density of 50,000 cells mL<sup>-1</sup> and incubated for 48 h. The supernatant was collected for cytokine profiling analysis, and then TRIZOL was added to extract RNA for further RNA-seq tests.

#### **Animal work**

Mice experiments comply with the relevant regulations, and all protocols are approved by the Institutional Animal Care and Use Committee, Zhejiang Academy of Medical Sciences (Approval number: ZJCLA-IACUC-20010236). Wild-type (WT) female C57BL/6 mice of 6–8 weeks in age were obtained from the animal center of Zhejiang Academy of Medical Sciences, S100a8-KO mice (Strain NO. T011976) were purchased from GemPharmatech (Nanjing, China). The animals were fed a standard laboratory diet and maintained with a 12-hour light/12-hour dark cycle.

For procedures in mice, the EVADE materials (H50, H70, and H90) and PDMS sheets were cut into discs with a biophysical punch (4 mm in diameter). Elastomers samples were sterilized with 75% ethanol, washed with normal saline, and implanted subcutaneously in C57BL/6 female mice. The implantation procedure was as follows. In brief, mice were anesthetized with 3% isoflurane in oxygen, shaved, and disinfected the skin with iodine. An 8 mm longitudinal incision was made on the dorsal surface using surgical scissors to access the subcutaneous space. Then subcutaneous pockets about 0.5 cm away from the incision were created with blunt forceps to implant the elastomer discs. After implantation, the incisions were closed using 5-0 taper-tipped PGA absorbable sutures. Mice were monitored until recovery from anesthesia and raised for 1 day, 2 weeks, 4 weeks, 3 months, 6 months, or longer, respectively. The mice grew normally without discomfort after the implantation, and no body weight loss was observed during the entire experiment.

NHP experiments comply with the relevant regulations, and all protocols are approved by the Laboratory Animal Ethics Committee of the Second Affiliated Hospital, School of Medicine, Zhejiang University (Approval number: 2023-No.30). Cynomolgus monkeys (male; 2 to 3 years old; 2 to 3.5 kg of body weight) were obtained from Suzhou Xishan Zhongke Laboratory Animal Co. Ltd., certified by the Association for Assessment and Accreditation of Laboratory Animal Care. The animals were fed a standard laboratory diet and maintained with a 12-hour light/12-hour dark cycle.

For procedures in NHPs, the animals were anesthetized via intramuscular injection of ketamine (5 mg/kg; Gutian Pharmaceutical) and midazolam (0.2 mg/kg; Ehwa Phrma) and ventilated with room air on an animal ventilator (Matrx, USA). Animals were kept on circulating warm water-based blankets and covered during the entire procedure for body temperature maintenance. An approximately 1 cm dorsal skin incision was made on the thoracic spine's left and right lateral sides. Blunt dissection was used to create a subcutaneous pocket ventrally about 5 cm deep. H90 and PDMS discs were placed on the left and right subcutaneous pockets. After implantation, the incisions were closed

using 5-0 taper-tipped PGA absorbable sutures. All animals received a single 50,000 U/kg perioperative penicillin G benzathine/ penicillin G procaine (Combi-Pen) injection and subcutaneous once-daily meloxicam (0.2 mg/kg on day 1 and 0.1 mg/kg on days 2 and 3) for postsurgical pain.

### Retrieval of tissues and elastomers

After two weeks, one month, three months, six months, or longer, mice were sacrificed, and the elastomer samples and the surrounding tissue were excised and collected. The explanted samples were either fixed in 10% formaldehyde solution (for use in histology) or flash frozen (for RNA or protein analysis).

For NHP SubQ retrievals, animal preparation for live excision procedures was carried out at the same time as implantation (described above). Then, biopsy punches (8 mm) were used to sample the skin and SC space at two-month retrieval time points. After retrieval, sites were closed with 5-0 taper-tipped PGA absorbable sutures.

### Immunostaining of tissue sections, microscopy, and quantitative image analysis

Tissue samples fixed in paraformaldehyde were dehydrated through a graded ethanol series and embedded in paraffin. Sections (3–5  $\mu\text{m}$ ) were cut using a microtome, deparaffinized in xylene, and rehydrated through sequential ethanol and distilled water baths. Sections were stained with hematoxylin, eosin (for cellularity), and Masson's trichrome (for collagen) following standard histological protocols. For immunohistochemistry, heat-induced epitope retrieval was performed using 0.1 M citrate buffer (pH 6) at 95 °C for 15 min. Sections were then rehydrated with three washes in PBS containing 0.1% Tween. Staining was conducted using a Diaminobenzidine (DAB) chromogenic reagent kit (DAKO, catalog no. K5007). Sections were blocked with peroxidase blocking solution for 10 min at room temperature and washed three times in PBS with 0.1% Tween. Primary antibodies targeting CCR-7 (rabbit IgG; 1:500; Abcam), TNF- $\alpha$  (goat IgG; 15  $\mu\text{g}/\text{mL}$ ; R&D Systems), IL-10 (goat IgG; 15  $\mu\text{g}/\text{mL}$ ; R&D Systems), IL-6 (goat IgG; 15  $\mu\text{g}/\text{mL}$ ; R&D Systems), S100a8 (rabbit IgG; 1:100; Solarbio), MRP8 + MRP14 (mouse IgG1; 1:100; Abcam),  $\alpha$ -SMA (mouse IgG2a; 1:400; Boster Bio), and F4/80 (rabbit IgG; 1:5,000; Abcam) were applied. Secondary antibodies conjugated with horseradish peroxidase (anti-mouse, anti-rabbit, or anti-goat) were used for detection. For immunofluorescence, sections were incubated in 0.1 M citrate buffer (pH 6) at 95 °C for 15 min and then rehydrated with three washes in TBS containing 0.025% Triton X-100. After incubation with 10% goat serum for 60 min, sections were exposed overnight to primary antibodies against F4/80 (rabbit IgG; 1:5,000; Abcam),  $\alpha$ -SMA (Cy3 polymer; mouse IgG2a; 3  $\mu\text{g}/\text{mL}$ ; Sigma), CD3 (Brilliant Violet 421 polymer; rat IgG2b; 3  $\mu\text{g}/\text{mL}$ ; BioLegend), and F4/80 (Alexa Fluor 647 polymer; rat IgG2a; 5  $\mu\text{g}/\text{mL}$ ; BioLegend). Detection was achieved using Alexa Fluor® 488-conjugated goat anti-rabbit IgG (H + L) F(ab')<sub>2</sub> Fragment (1:200; Cell Signaling Technology) and nuclei were stained with 4',6-diamidino-2-phenylindole (DAPI; 1:50; Sigma-Aldrich). Images were captured with a Nikon intensilight CHGFI microscope and NIS-Elements AR software, and analyzed using a Virtual Slide Microscope (VS120-S6-W, Olympus). Capsule thickness was defined as collagen-rich tissue between the implant surface and adjacent structures. Collagen thickness was quantified from Masson's trichrome-stained sections. Positive staining areas for TNF- $\alpha$ , IL-6, CCR-7, IL-10, S100a8,  $\alpha$ -SMA, and F4/80 were calculated as percentages using ImageJ. All images were processed with Adobe Photoshop 2023, with consistent adjustments to contrast and brightness for representative images.

### Protein extraction

Proteins were extracted from skin tissue surrounding H90 implants, PDMS, and non-implanted tissue for further analysis. RIPA lysis buffer (containing phenylmethylsulfonyl fluoride) from Solarbio (catalog no.

R0010) was added to the isolated tissue. The tissue was homogenized and lysed on ice for 30 min. Following lysis, the sample was centrifuged at 10,000 g for 5 min at 4 °C, and the supernatant was collected. Protein concentration was determined using a BCA kit from Beyotime (catalog no. P0010S). The protein extract was aliquoted and stored at –80 °C for subsequent use.

### Cytokine profiling analysis

A proteome profiler antibody array from the R&D System (catalog no. ARY006) was used for cytokine profiling. After two weeks of implantation, tissue samples were excised and collected, using a mock group without implantation as control. Proteins from the above tissue samples were extracted. Next, 2 mL of blocking buffer was pipetted into each well of the 4-well multi-dish containing each antibody array membrane and incubated for 1 h on a rocking platform shaker. The blocking buffer was aspirated, and 1.5 mL sample solutions containing 300  $\mu\text{g}$  proteins and 15  $\mu\text{L}$  detection antibody cocktail were pipetted to each well and incubated overnight at 2–8 °C on a shaker. Each membrane was carefully placed into individual plastic containers and washed three times with a wash buffer. The membrane was put into the 4-well multidish, containing 2 mL diluted Streptavidin-HRP (1:2,000), and incubated for 30 min on a shaker. After washing three times by wash buffer, the membranes were incubated with 1 mL of Chemi Reagent Mix for 1 min and placed in an autoradiography film cassette (ChemiScope 6000, Clinx) for chemiluminescence. The gray value was measured using ImageJ software.

### scRNA-seq analysis

PDMS and H90 discs were implanted into the subcutaneous space of the mice. After one week, implants were removed and washed with sterile PBS to isolate cells from the surface. The resulting cells were pooled per condition and sorted on a Sony MA900 Cell Sorter to filter out dead cells. Libraries were generated from the remaining cells on the DNBelab C4 system according to the manufacturer's instructions. The barcode sequencing libraries were quantified by Qubit (Invitrogen). The sequencing libraries were sequenced using the DIPSEQ T1 sequencer at the China National GeneBank. The R package Seurat V4 (Satija Lab) was used to cluster the transcripts using K-means clustering and generate UMAP coordinates, visualized on the Loupe Browser 6.0. Clusters were identified as immune cell populations by expression of common immune cell markers, Fnl1&Csflr (macrophages), T/NK cells (Cd3d&Prfl), and dendritic cells (Flt3).

### RNA-seq and data analysis

Total RNA was extracted from skin tissue near the implants using TRIzol reagent and treated with an RNase-Free DNase Set (Qiagen). Quantitative RT-PCR was performed with Power SYBR Green Master Mix (Applied Biosystems) following the manufacturer's guidelines. Extracted RNA (500 ng) was reverse transcribed into complementary DNA (cDNA) using SuperScript™ III First-Strand Synthesis SuperMix (Thermo Fisher). qRT-PCR was conducted on a Real-Time PCR Detection System (CFX384, Bio-Rad, USA) using recommended settings for quantitative and relative expression. Primer sequences used for qRT-PCR are detailed in Supplementary Table 3.

### Western blotting

Protein was extracted from skin tissue near the implants by using T-PER Tissue Protein Extraction Reagent (catalog no. 78510, Thermo Pierce) with protease inhibitors (Halt Protease inhibitor single-use cocktail, catalog no. 78445, Thermo Pierce) on ice, and then lysed by sonication (for 30 s on, 30 s off, twice at 70% amplitude). Samples were then subjected to constant agitation for 2 h at 4 °C. Lysates were then centrifuged for 20 min at 7200 g at 4 °C, and protein-containing supernatants were collected in fresh tubes kept on ice. In samples from fat tissue, an excess of fat (a top layer on the supernatant) was first

removed before supernatant transfer. 20 µg protein (quantified by BCA assay, BCA protein assay kit, catalog no. P0010, Beyotime) for each lane was boiled at 95 °C for 5 min and electrophoresed on SDS-polyacrylamide gels (Any kD 15-well comb mini-gel, Biorad, catalog no. 456-9036) and then blotted onto nitrocellulose membranes (Millipore, catalog no. IPVH00010). Blots were probed with anti-S100a8 antibody (1:500 dilution; rabbit polyclonal to S100a8; catalog no. 15792-1; Proteintech), anti-IL-17 antibody (1:500 dilution; mouse monoclonal to IL-17; catalog no. 66148-1; Proteintech), anti-IL-1β antibody (1:1,000 dilution; rabbit monoclonal to IL-1β; catalog no. ab254360; Abcam), and anti-TNF-α antibody (1:1,000 dilution; rabbit polyclonal to TNF-α; catalog no. ab6671; Abcam) and anti-β-actin antibody (1:4,000 dilution; monoclonal anti-β-actin antibody produced in mouse; catalog no. A1978; Sigma Aldrich), and anti-GAPDH antibody (1:10,000 dilution; monoclonal anti-GAPDH antibody produced in rabbit; catalog no. ab181602; Abcam) as loading controls followed by goat anti-mouse (1:5000 dilution; catalog no. 62-6520; Thermo Fisher) and goat anti-rabbit (1:10,000 dilution; catalog no. 31460; Thermo Fisher) HRP-conjugated secondary antibodies. Antibody-antigen complexes were visualized using SuperSignal™ West Dura (Thermo Fisher, catalog no. 34075).

### Quantitative PCR assay

Total RNA was isolated from skin tissue adjacent to the implants using TRIzol reagent and an RNase-Free DNase Set (Qiagen). Complementary DNA (cDNA) was synthesized from 500 ng of RNA with a SuperScript™ III First-Strand Synthesis SuperMix (Thermo Fisher). Quantitative real-time PCR (qRT-PCR) was performed with Power SYBR Green Master Mix (Applied Biosystems) following the manufacturer's guidelines. qRT-PCR was carried out on a Real-Time PCR Detection System (CFX384, Bio-Rad, USA), using the recommended settings for quantitative and relative expression analysis. The primers used are detailed in Supplementary Table 3.

### Interleukin-17 (IL-17) and glyceraldehyde-3-phosphate dehydrogenase (GAPDH)'s relative levels tested by enzyme-linked immunosorbent assay (ELISA)

An IL-17 ELISA kit from Absin (catalog no. 520009) was used to test the concentration of IL-17 in extracted protein samples. After the implantation of elastomers for one month, tissue samples from implantation were excised and collected. The tissue protein was extracted using a mock group without implantation as a control. In brief, 35 µg extracted protein solutions were added to 96-well plates pre-coated with capture antibody and incubated for 2 h, followed by three washes with wash buffer. The detection antibody was then added to plates and incubated for 2 h, followed by three washes with wash buffer. Next, the streptavidin-HRP was added to plates and incubated for 20 min, followed by three washes with washing buffer. Finally, the 3, 3', 5, 5'-tetramethylbenzidine (TMB) chromogen solution was added to the plates. After 20 min incubation, the enzymatic reaction was stopped by adding an equal volume of 2 N H<sub>2</sub>SO<sub>4</sub>. Absorbance values at 450 nm and 540 nm (as calibration wavelength) were recorded by a microplate reader (MODEL 550, Bio-Rad). Average data were acquired from five specimens.

At the same time, the concentration of GAPDH was measured to correct the experimental results. After the implantation of elastomers for one month, tissue samples from implantation were excised and collected, using a mock group without implantation as the control. In brief, the 96-well plate was incubated with a capture antibody from Beyotime (dilution 1:3,000; catalog no. AG019) overnight at 4 °C, followed by three washes with wash buffer. 10 µg extracted protein samples were added to the plate and incubated for 2 h, followed by 3 washes with wash buffer. Afterward, the plate was incubated with HRP-conjugated detection antibody from Proteintech (dilution 1:50,000; catalog no. 60004) for 2 h, followed by 3 washes with wash buffer.

Finally, a TMB chromogen solution was added to the plates. After 20 min incubation, the enzymatic reaction was stopped by adding an equal volume of 2 N H<sub>2</sub>SO<sub>4</sub>. Absorbance values at 450 nm and 540 nm (as calibration wavelength) were recorded by a microplate reader (MODEL 550, Bio-Rad). Average data were acquired from five specimens.

### Surface protein analysis of elastomers

The in vitro fibrinogen adsorption and in vivo protein adsorption 24-hour post-implantation of EVADE and PDMS elastomers were investigated.

### Fibrinogen fouling test by enzyme-linked immunosorbent assay (ELISA)

Fibrinogen (Fg) was selected as the test protein to examine the anti-fouling property of the EVADE elastomer samples (H50, H70, and H90). In brief, EVADE materials were cut from the 1 mm thick elastomer sheet into 4 mm diameter discs with a biopuncher. In addition, a 1 mm thick PDMS sheet and 2-methacryloyloxyethyl phosphorylcholine (MPC) hydrogel sheet were cut into 4 mm diameter discs with a biopuncher and used as controls. To make MPC hydrogels, 200 mg MPC and 20 mg MBAA were dissolved in 1 mL distilled water followed by the addition of 4 mg APS and 4 µL TEMED. After the vortex, the solution was immediately injected into the mold and reacted for 24 h. The resulting hydrogels were soaked in PBS (pH 7.4) for 48 h to remove the residual small molecules. The samples were first placed in a 24-well plate and incubated in PBS for 5 min to equilibrate. Next, the samples were incubated with 1 mL of 1 mg mL<sup>-1</sup> Fg in PBS buffer for 1 h, followed by 3 washes with PBS buffer. Samples were then transferred to new wells and incubated with 1 mL of horseradish peroxidase (HRP) conjugated anti-fibrinogen (1 µg mL<sup>-1</sup>) from Bellancom Chemistry (catalog no. G11390) in PBS buffer for 0.5 h. All samples were then transferred to new wells after another five washes with pure PBS buffer. Afterward, 1 mL of OPD chromogen solution was added. After 15 min incubation, the enzymatic reaction was stopped by adding an equal volume of 1 N HCl. The absorbance value at 490 nm was recorded by a microplate reader (MODEL 550, Bio-Rad) and was normalized to that of the PDMS sample. Average data were acquired from six specimens.

**Proteomics.** After the elastomers were implanted subcutaneously for 24 h, remove them from the body, peel off the visible attached tissue, gently rinse with PBS, and store at -80 °C. For this assay, proteins adsorbed on the elastomer surface were reduced (5 mM dithiothreitol; 56 °C for 30 min) and alkylated (11 mM iodoacetamide; room temperature in the dark for 15 min). Trypsin was added at 1:50 trypsin-to-protein mass ratio for the first digestion overnight and 1:100 trypsin-to-protein mass ratio for a second 4 h-digestion. The digested peptides were desalted by a Strata X C18 column (Phenomenex, Torrance, CA, USA) and lyophilized. The peptides were labeled based on the manufacturing instructions of the TMTsixplex (Thermo Fisher Scientific). Tryptic peptides were separated by high-pH reversed-phase high-performance liquid chromatography (HPLC) using an Agilent 300Extend C18 column (5 µm particle size, 4.6 mm inner diameter, 250 mm length; Agilent, Fremont, CA, USA). Peptide samples were analyzed using an EASY-nLC 1000 LC system (Thermo Fisher Scientific, Waltham, MA, USA) coupled with an Orbitrap Fusion mass spectrometer (Thermo Fisher Scientific) and subsequently analyzed on a Q Exactive Plus mass spectrometer (Thermo Fisher Scientific). MS/MS files were searched against the UniProt human proteome database (20380 sequences) using MaxQuant (version 1.5.2.8) software enabled with the Andromeda search engine. The quantification analysis was performed at the protein level by MaxQuant software. Peptides were desalted using C18 SpinTips (Protea) then lyophilized and stored at -80 °C. Per the manufacturer's instructions, peptides were labeled with TMTsixplex (Thermo Fisher Scientific). Peptides were then loaded on a pre-column and separated by reverse-phase high-performance

liquid chromatography (Easy nLC 1000; Thermo Fisher Scientific) over a 140-min gradient before nano-electrospray using a Q Exactive mass spectrometer (Thermo Fisher Scientific). Raw mass spectral data files were searched using Proteome Discoverer (Thermo Fisher Scientific) and Mascot version 2.4.1 (Matrix Science). Tandem mass tag (TMT) quantification was obtained using Proteome Discoverer and isotopically corrected per the manufacturer's instructions.

### Mice models of inhibiting and knocking out of S100A8/S100A9

Two mice models were constructed to confirm the relationship between S100A8/A9 expression and the FBR.

**Inhibition of S100A9 with tasquinimod.** For mice implanted with PDMS, the distribution of tasquinimod at 1 mg/kg/day and 3 mg/kg/day (administered orally via drinking water) started the day after implantation and continued for one month.

**Generation of S100A8 conditional knockout (cKO) mice.** In brief, S100a8 conditional knockout homozygote (cHO) mice (Lyz2-iCre<sup>+/-</sup>, S100a8<sup>fl/fl</sup>) were produced by crossing S100a8 conditional knockout heterozygote (cHE) mice (Lyz2-iCre<sup>+/-</sup>, S100a8<sup>fl/+</sup>) with homozygous S100a8 floxed mice (Lyz2-iCre<sup>-/-</sup>, S100a8<sup>fl/fl</sup>). Both S100a8-CKO (Strain NO. T011059) and Lyz2-iCre (Strain NO. T003822) were purchased from GemPharmatech (Nanjing, China). S100a8 cHO mice were generated through two rounds of crossing: homozygous S100a8-CKO mouse (S100a8<sup>fl/fl</sup>) × Cre-positive mouse (Lyz2-iCre<sup>+/-</sup>), and then crossing with the resulting heterozygous S100a8 cHE mice (Lyz2-iCre<sup>+/-</sup>, S100a8<sup>fl/+</sup>).

### Diabetes induction in mice

Wild-type (WT) male C57BL/6 mice, aged 6–8 weeks, were sourced from the Zhejiang Academy of Medical Sciences animal center. To induce diabetes, mice were given daily intraperitoneal injections of 50 mg/kg body weight STZ (10 mg/mL in citrate buffer, pH 4.5) for five consecutive days while maintaining a non-fasted regular diet. Fourteen days post-injection, body weight and blood glucose levels were assessed to confirm diabetes. Mice with non-fasted blood glucose levels exceeding 19.4 mmol/L for two consecutive days were deemed diabetic.

### Fabrication of EVADE CSII catheter

To prepare the EVADE CSII catheter, a stainless steel wire with a diameter of 400 μm was immersed in sucrose solution and dried to form a soluble layer, facilitating easy demolding. Subsequently, the wire was soaked in a reaction mixture containing HPMA monomer, ODA monomer, and 0.5 wt% (relative to the weight of monomers) of photoinitiator Irgacure 819. The stainless steel surface was then dip-coated with this mixture to form a uniform polymer solution layer at a speed of 10 mm/min. Polymerization occurred under UV irradiation (365 nm) at approximately 180 mW/cm<sup>2</sup> for 10 min. After polymerization, the elastomer samples were immersed in a sterile PBS buffer (pH 7.4) for two days, demolding and drying under vacuum at room temperature. Subsequently, the catheter was cut from the infusion set, and adhesive was used to affix the EVADE CSII catheter onto the infusion set.

### In vivo insulin infusion catheter implantation in mice

Diabetic C57BL/6 mice were shaved and anesthetized using 3% isoflurane in oxygen, shaved, and disinfected the skin with iodine. A longitudinal incision of about 4 mm was made on the dorsal surface using surgical scissors to provide access to the subcutaneous space. Then subcutaneous pockets about 0.5 cm away from the incision were created with blunt forceps to implant the catheters. After implantation, the incisions were closed using 5-0 taper-tipped PGA absorbable sutures. Mice were monitored until recovery from anesthesia and raised for one month. The mice grew normally without discomfort

after the implantation, and no body weight loss was observed during the entire experiment.

### Insulin pump therapy in mice

Diabetic mice with newly induced diabetes had their dorsal skin shaved and disinfected with iodine. An infusion catheter was then inserted subcutaneously. To evaluate the performance of EVADE CSII catheters under natural micromotion, the catheter was connected to an infusion line and the mouse was allowed to wear the complete infusion set, including the catheter and line, for up to 7 days without restriction in a single cage. For assessing continuous insulin infusion via EVADE CSII catheters, the infusion set was connected to an insulin pump (Medtronic MiniMed 722) filled with 0.2 IU/mL insulin. Mice received a continuous basal insulin infusion at a rate of 10 μL/h, with three additional bolus insulin infusions of 45 μL each. On day seven post-catheter insertion, an insulin absorption assay was performed by administering a bolus infusion of 2 IU/kg insulin through the pump. Blood glucose levels were measured at predefined intervals using a glucometer following insulin infusion. Serum insulin levels were determined by centrifuging blood samples (3000 × g, 4 °C) for 15 min, followed by quantification with the Elabscience human insulin ELISA kit (E-EL-H2665). Throughout the study, mice were fasted but had ad libitum access to water. Mice receiving subcutaneous insulin injections at the same dosage served as controls.

### Statistics and reproducibility

Details of the sample size and appropriate statistical test are included in the figure captions. The data are expressed as means ± s.d. The data were analyzed for statistical significance by two-side one-way analysis of variance (ANOVA) with Bonferroni multiple comparison correction or unpaired, two-tailed *t*-test using SPSS Statistics 26.0. No adjustments were made for multiple comparisons. All in vitro and in vivo results are representative of three to six independents.

### Reporting summary

Further information on research design is available in the Nature Portfolio Reporting Summary linked to this article.

### Data availability

All relevant data supporting the key findings of this study are available within the article and its Supplementary Information files. Source data are provided with this paper. Source data is available for Fig. 1b, Fig. 1c, Fig. 1d, Fig. 1g, Fig. 1h, Fig. 1j, Fig. 2b, Fig. 2d, Fig. 2j, Fig. 3f, Fig. 3g, Fig. 3h, Fig. 4a, Fig. 4b, Fig. 4c, Fig. 4e, Fig. 4f, Fig. 4g, Fig. 4j, Fig. 4m, Fig. 4o, Fig. 4p, Fig. 5b, Fig. 5c, Fig. 5f, Fig. 5g, Fig. 6c, Fig. 6d, and Fig. 6e in the associated source data file. The mass spectrometry proteomics data have been deposited to the ProteomeXchange Consortium via the PRIDE partner repository with the dataset identifier PXD054629. RNA-Seq data were deposited at National Center for Biotechnology Information Gene Expression Omnibus (GEO) with accession number GSE275010. Source data are provided with this paper.

### References

- Li, J. et al. A tissue-like neurotransmitter sensor for the brain and gut. *Nature* **606**, 94–101 (2022).
- Madhvapathy, S. R. et al. Implantable bioelectronic systems for early detection of kidney transplant rejection. *Science* **381**, 1105–1112 (2023).
- Hu, L. et al. An implantable soft robotic ventilator augments inspiration in a pig model of respiratory insufficiency. *Nat. Biomed. Eng.* **7**, 110–123 (2023).
- Hung, H. C. et al. A coating-free nonfouling polymeric elastomer. *Adv. Mater.* **29**, 1700617 (2017).
- Wu, N. et al. Electrode materials for brain-machine interface: a review. *InfoMat* **3**, 1174–1194 (2021).

6. Choi, Y. S. et al. Fully implantable and bioresorbable cardiac pacemakers without leads or batteries. *Nat. Biotechnol.* **39**, 1228–1238 (2021).
7. Yi, Z. et al. A battery-and leadless heart-worn pacemaker strategy. *Adv. Funct. Mater.* **30**, 2000477 (2020).
8. Zhang, E. et al. An injectable and biodegradable zwitterionic gel for extending the longevity and performance of insulin infusion catheters. *Nat. Biomed. Eng.* <https://doi.org/10.1038/s41551-023-01108-z> (2023).
9. Jensen, M. J. et al. Cochlear implant material effects on inflammatory cell function and foreign body response. *Hear. Res.* **426**, 108597 (2022).
10. Villarruel Mendoza, L. A. et al. Recent advances in micro-electro-mechanical devices for controlled drug release applications. *Front. Bioeng. Biotechnol.* **8**, 827 (2020).
11. Doloff, J. C. et al. The surface topography of silicone breast implants mediates the foreign body response in mice, rabbits and humans. *Nat. Biomed. Eng.* **5**, 1115–1130 (2021).
12. Karinja, S. J. et al. An anti-fibrotic breast implant surface coating significantly reduces peri-prosthetic capsule formation. *Plast. Reconstr. Surg.* **152**, 775–785 (2023).
13. Zhou, X. et al. Covalently grafted human serum albumin coating mitigates the foreign body response against silicone implants in mice. *Bioact. Mater.* **34**, 482–493 (2024).
14. Liu, Z. et al. Fibrous capsule-resistant, controllably degradable and functionalizable zwitterionic-albumin hybrid hydrogels. *Biomater. Sci.* **12**, 468–478 (2024).
15. Farah, S. et al. Long-term implant fibrosis prevention in rodents and non-human primates using crystallized drug formulations. *Nat. Mater.* **18**, 892–904 (2019).
16. Doloff, J. C. et al. Colony stimulating factor-1 receptor is a central component of the foreign body response to biomaterial implants in rodents and non-human primates. *Nat. Mater.* **16**, 671–680 (2017).
17. Noskovicova, N. et al. Suppression of the fibrotic encapsulation of silicone implants by inhibiting the mechanical activation of pro-fibrotic TGF- $\beta$ . *Nat. Biomed. Eng.* **5**, 1437–1456 (2021).
18. Liu, Q. et al. A zwitterionic polyurethane nanoporous device with low foreign-body response for islet encapsulation. *Adv. Mater.* **33**, 2102852 (2021).
19. Wang, X. et al. A nanofibrous encapsulation device for safe delivery of insulin-producing cells to treat type 1 diabetes. *Sci. Transl. Med.* **13**, eabb4601 (2021).
20. Zhou, X. et al. Materials strategies to overcome the foreign body response. *Adv. Healthc. Mater.* **13**, 2304478 (2024).
21. Zhang, D. et al. Dealing with the foreign-body response to implanted biomaterials: strategies and applications of new materials. *Adv. Funct. Mater.* **31**, 2007226 (2021).
22. Chandorkar, Y. et al. The foreign body response demystified. *ACS Biomater. Sci. Eng.* **5**, 19–44 (2019).
23. Kim, Y. K. et al. Biomolecular strategies to modulate the macrophage response to implanted materials. *J. Mater. Chem. B* **4**, 1600–1609 (2016).
24. Liu, Q. et al. Zwitterionically modified alginates mitigate cellular overgrowth for cell encapsulation. *Nat. Commun.* **10**, 5262 (2019).
25. Zhang, L. et al. Zwitterionic hydrogels implanted in mice resist the foreign-body reaction. *Nat. Biotechnol.* **31**, 553–556 (2013).
26. Dong, D. et al. High-strength and fibrous capsule-resistant zwitterionic elastomers. *Sci. Adv.* **7**, eabc5442 (2021).
27. Bochenek, M. A. et al. Alginate encapsulation as long-term immune protection of allogeneic pancreatic islet cells transplanted into the omental bursa of macaques. *Nat. Biomed. Eng.* **2**, 810–821 (2018).
28. Veiseh, O. et al. Domesticating the foreign body response: recent advances and applications. *Adv. Drug Delivery Rev.* **144**, 148–161 (2019).
29. Zhang, D. et al. Bio-inspired poly-DL-serine materials resist the foreign-body response. *Nat. Commun.* **12**, 5327 (2021).
30. Zhang, D. et al. Silk-Inspired  $\beta$ -peptide materials resist fouling and the foreign-body response. *Angew. Chem. Int. Ed.* **132**, 9673–9680 (2020).
31. Zhou, X. et al. Poly(Glutamic Acid-Lysine) hydrogels with alternating sequence resist the foreign body response in rodents and non-human primates. *Adv. Sci.* **11**, 2308077 (2024).
32. Padmanabhan, J. et al. Allometrically scaling tissue forces drive pathological foreign-body responses to implants via Rac2-activated myeloid cells. *Nat. Biomed. Eng.* **7**, 1419–1436 (2023).
33. Yuk, H. et al. Hydrogel interfaces for merging humans and machines. *Nat. Rev. Mater.* **7**, 935–952 (2022).
34. Pakshir, P. et al. Controlled release of low-molecular weight, polymer-free corticosteroid coatings suppresses fibrotic encapsulation of implanted medical devices. *Biomaterials* **286**, 121586 (2022).
35. Brandt, C. J. et al. Beneficial effects of hydrocortisone or spironolactone coating on foreign body response to mesh biomaterial in a mouse model. *J. Biomed. Mater. Res. A* **99**, 335–343 (2011).
36. Kang, S. et al. Efficient reduction of fibrous capsule formation around silicone breast implants densely grafted with 2-methacryloyloxyethyl phosphorylcholine (MPC) polymers by heat-induced polymerization. *Biomater. Sci.* **8**, 1580–1591 (2020).
37. Li, Q. et al. Zwitterionic biomaterials. *Chem. Rev.* **122**, 17073–17154 (2022).
38. Yan, H. et al. Immune-informed mucin hydrogels evade fibrotic foreign body response in vivo. *Adv. Funct. Mater.* **29**, 1902581 (2019).
39. Bose, S. et al. A retrievable implant for the long-term encapsulation and survival of therapeutic xenogeneic cells. *Nat. Biomed. Eng.* **4**, 814–826 (2020).
40. Schreiber, C. C. et al. Lipid deposition profiles influence foreign body responses. *Adv. Mater.* **35**, 2205709 (2023).
41. Vegas, A. J. et al. Combinatorial hydrogel library enables identification of materials that mitigate the foreign body response in primates. *Nat. Biotechnol.* **34**, 345–352 (2016).
42. Mukherjee, S. et al. Screening hydrogels for antifibrotic properties by implanting cellularly barcoded alginates in mice and a non human primate. *Nat. Biomed. Eng.* **7**, 867–886 (2023).
43. Rostam, H. M. et al. Immune-instructive polymers control macrophage phenotype and modulate the foreign body response in vivo. *Matter* **2**, 1564–1581 (2020).
44. Doloff, J. C. et al. Identification of a humanized mouse model for functional testing of immune-mediated biomaterial foreign body response. *Sci. Adv.* **9**, eade9488 (2023).
45. Goswami, R. et al. Mechanosensing by TRPV4 mediates stiffness-induced foreign body response and giant cell formation. *Sci. Signal.* **14**, eabd4077 (2021).
46. Veiseh, O. et al. Size-and shape-dependent foreign body immune response to materials implanted in rodents and non-human primates. *Nat. Mater.* **14**, 643–651 (2015).
47. Kyriakides, T. R. et al. Foreign body response to synthetic polymer biomaterials and the role of adaptive immunity. *Biomed. Mater.* **17**, 022007 (2022).
48. Chung, L. et al. Interleukin 17 and senescent cells regulate the foreign body response to synthetic material implants in mice and humans. *Sci. Transl. Med.* **12**, eaax3799 (2020).
49. Shen, M. et al. The effects of surface chemistry and adsorbed proteins on monocyte/macrophage adhesion to chemically modified polystyrene surfaces. *J. Biomed. Mater. Res.* **57**, 336–345 (2001).
50. Zhou, X. et al. An elastomer with in situ generated pure zwitterionic surfaces for fibrosis-resistant implants. *Acta Biomater.* <https://doi.org/10.1016/j.actbio.2024.06.047> (2024).



51. Loser, K. et al. The Toll-like receptor 4 ligands Mrp8 and Mrp14 are crucial in the development of autoreactive CD8<sup>+</sup> T cells. *Nat. Med.* **16**, 713–717 (2010).
52. Leclerc, E. et al. Binding of S100 proteins to RAGE: an update. *Biochim. Biophys. Acta. Mol. Cell. Res.* **1793**, 993–1007 (2009).
53. Wang, S. et al. S100A8/A9 in inflammation. *Front. Immunol.* **9**, 1298 (2018).

## Acknowledgements

This work was financially supported by the National Natural Science Foundation of China (52103188 to P.Z., 22175152 to P.Z.), the Huadong Medicine Joint Funds of the Zhejiang Provincial Natural Science Foundation of China (LHDMZ22H300011 to P.Z.), the National Key Research and Development Program of China (2022YFB3807300 to P.Z.), the financial support from State Key Laboratory of Transvascular Implantation Devices (012024019 to P.Z.), and the Fundamental Research Funds for the Central Universities (226-2024-00086 to P.Z.).

## Author contributions

P.Z. conceived the overall project. X.Z., Zuolong Liu, and F.J. designed the elastomer synthesis approach. X.Z. synthesized the elastomers. X.Z., W.C., and Z.Z. performed the mice studies. X.Z., Y.C., and Y.N. performed the in vitro studies. X.Z. analyzed the histology samples. X.Z., Zhouyu Lu, and Y.Y. performed the cynomolgus monkey studies. H.H., K.Y., and W.L. supervised the cynomolgus monkey study and helped in data analysis. X.Z. and P.Z. designed the experiments, interpreted the data, and wrote the manuscript. Y.W., J.J., and P.Z. supervised the study. All authors discussed the results and commented on the manuscript.

## Competing interests

P.Z., J.J., and X.Z. are inventors of a patent related to this work filed by Zhejiang University (ZL 202310321856.8), the remaining authors declare no competing interest.

## Additional information

**Supplementary information** The online version contains supplementary material available at <https://doi.org/10.1038/s41467-024-52023-z>.

**Correspondence** and requests for materials should be addressed to Peng Zhang.

**Peer review information** *Nature Communications* thanks the anonymous reviewers for their contribution to the peer review of this work. A peer review file is available.

**Reprints and permissions information** is available at <http://www.nature.com/reprints>

**Publisher's note** Springer Nature remains neutral with regard to jurisdictional claims in published maps and institutional affiliations.

**Open Access** This article is licensed under a Creative Commons Attribution-NonCommercial-NoDerivatives 4.0 International License, which permits any non-commercial use, sharing, distribution and reproduction in any medium or format, as long as you give appropriate credit to the original author(s) and the source, provide a link to the Creative Commons licence, and indicate if you modified the licensed material. You do not have permission under this licence to share adapted material derived from this article or parts of it. The images or other third party material in this article are included in the article's Creative Commons licence, unless indicated otherwise in a credit line to the material. If material is not included in the article's Creative Commons licence and your intended use is not permitted by statutory regulation or exceeds the permitted use, you will need to obtain permission directly from the copyright holder. To view a copy of this licence, visit <http://creativecommons.org/licenses/by-nc-nd/4.0/>.

© The Author(s) 2024